Positronium Bloch Function, and Trapping of Positronium in Vacancies, in Ice

Mogensen, O.E.; Eldrup, M.

Publication date:
1977

Document Version
Publisher's PDF, also known as Version of record

Risø Report No. 366

Risø Report No. 366

Risø National Laboratory

Positronium Bloch Function, and Trapping of Positronium in Vacancies, in Ice

by O. E. Mogensen and M. Eldrup

August 1977

Sales distributors: Jul. Gjellerup, Sølvgade 87, DK-1307 Copenhagen K, Denmark

Available on exchange from: Risø Library, Risø National Laboratory, DK-4000 Roskilde, Denmark

INIS descriptors

ANGULAR CORRELATION
ANNIHILATION
BLOCH THEORY
COMPUTER CALCULATIONS
DIELECTRICAL PROPERTIES
GAUSS FUNCTION
ICE
LIFETIME
LOW TEMPERATURE
MOLECULAR CRYSTALS
MONOCRYSTALS
POSITRONIUM
POSITRONS
TEMPERATURE DEPENDENCE
TRAPPING
VANCIES
WATER

UDC 539.124.6 : 539.189.2 : 546.212-162

August 1977 Risø Report No. 366

Positronium Bloch Function, and Trapping of Positronium in Vacancies, in Ice

by

O.E. Mogensen and M. Eldrup

Risø National Laboratory
Chemistry Department

Abstract

Positron annihilation techniques (PAT) were used to study the behaviour of positronium (Ps) in pure H_2O and D_2O ice in the temperature interval $-185 \leq t \leq 2^{\circ}C$. At temperatures below roughly $-100^{\circ}C$, the linear-slit angular correlation curves consisted of a broad component (fwhm ≈ 10.5 mrad), resulting from free positron and Ps pick-off annihilation, and narrow central and side peaks (fwhm ≈ 1 mrad), resulting from intrinsic para-Ps annihilation from a center-of-mass Bloch-function state. At higher temperatures there also occurred a middle-broad component (fwhm ≈ 3.9 mrad) resulting from intrinsic para-Ps annihilation from a localized Ps state. Positron lifetime measurements on pure ice gave an ortho-Ps pick-off lifetime of 0.66 nsec at low temperatures, which above $-100^{\circ}C$ increased to about 1.0 nsec at the melting point, in agreement with previous measurements. This increase in ortho-Ps lifetime and the middle-broad angular correlation component are believed to be caused by Ps trapping by temperature created vacancies. A weak long-lifetime component ($\sim$2 nsec) present at higher temperatures is ascribed to Ps trapping in divacancies. The theory of

the 2-γ annihilation of a Ps many-electron system is discussed. Two new "exchange" terms in the annihilation probability were derived, and it was shown that the para-Ps pick-off annihilation rate is smaller than that of ortho-Ps. The square of the numerical value of the Fourier transform at various reciprocal lattice points of the Ps Bloch function, $|a_{\vec{q}}|^2$, was extracted by very detailed computer analyses. A nearly-free-Ps theory, taking into account the influence of phonons, could not explain the temperature dependence of $|a_{\vec{q}}|^2$. The Ps trapping in vacancies could not be explained in detail in terms of several models, including the simple "trapping model". The main difficulty was the fact that para-Ps and ortho-Ps are trapped at roughly the same amount at a certain vacancy concentration. Our results imply a high (several ppm) vacancy concentration at the melting point in ice in agreement with other independent estimates. This fact might introduce pronounced changes in currently accepted theories of the electrical properties of ice.

ISBN 87-550-0488-1

CONTENTS

		Page
1.	Introduction	5
2.	Experimental	7
3.	Data Analysis and Results	9
	3.1. Measurements	9
	3.2. Lifetime Spectra: Analysis and Results	13
	3.3. Analysis of the Angular Correlation Curves	15
	3.4. Reciprocal Lattice Point Contributions	23
4.	Theory	27
	4.1. General Remarks	27
	4.2. Annihilation Probability	28
	4.3. Models of the Positronium State	35
5.	Discussion	41
	5.1. General Remarks	41
	5.2. Evidence for Positronium in Ice	42
	5.3. Positronium Yield in Ice	43
	5.4. The Positronium Bloch Function	48
	5.5. Positronium Trapping in Vacancies	51
	5.5.1. Introductory Remarks	51
	5.5.2. The Trapping Model	52
	5.5.3. Linear Combination Model	57
	5.5.4. Concluding Remarks	58
	5.6. Vacancies in Ice	59
	5.7. Miscellaneous Remarks	61
6.	Summary and Conclusion	62
Acknowledgements		67
References		68

1. INTRODUCTION

A positron entering a solid or a liquid will normally be slowed down to thermal velocities within a very short time ($\leq$ 1 psec). After a period (the positron lifetime) it will annihilate with an electron and normally two γ-quanta are emitted. These annihilation photons carry information about the electron-positron state at the moment of annihilation. Hence, experimental studies of the photons may give useful information about the physical and chemical structure of the material under investigation.

Three experimental methods are mainly used in PAT (i.e. Positron Annihilation Technique)[1-6]. They measure a) the distribution of positron lifetimes, b) the angular correlation between the two annihilation photons, and c) the Doppler broadening of one of the annihilation photons. The first two methods were used in the present work.

In recent years PAT has been used to investigate defect properties in metals, and it is now accepted as an important new tool in basic studies of metal defects[3,7]. The changes in the properties of the annihilation photons caused by positron trapping in vacancy-type defects are measured. Positrons are sensitive to parts per million (ppm) concentrations of vacancies. PAT is probably the only method available for a detailed study of small ($\leq$ 15 Å) three dimensional vacancy clusters (voids) in metals[8], and for a determination of vacancy formation energies in refractory and impure metals. Also defects in ionic crystals (F-centers, cation vacancies, etc.) can be studied by use of PAT[3,9].

The hydrogen-like bound state of a positron and an electron, positronium (Ps), is formed before annihilation takes place in various molecular liquids and solids and in some ionic crystals, but not in metals and semiconductors. Ortho-Ps pick-off annihilation with the outer electrons of the molecules gives rise to a long-lifetime component in the lifetime spectra, while the presence of a narrow component in the angular correlation distributions can be ascribed to intrinsic para-Ps annihilation. The ortho-Ps pick-off lifetime is strongly decreased if Ps takes part in a chemical reaction, while it is increased in the case of a Ps trapping in holes (vacancy, vacancy clusters, etc.) in

a crystal. Hence, also the behaviour of Ps can be studied by use of PAT.

One purpose of the present work was a PAT-study of defects in ice. About 73% of the positrons form Ps in ice. Our results show that Ps is trapped in defects in ice at higher temperatures and in impurity-doped ice. Our interpretation of the results is that Ps is mainly trapped in vacancies (missing H_2O molecules). Apart from indirect evidence (mainly selfdiffusion results[10-17]), vacancies in ice seem not to have been studied earlier.

Although it is generally accepted[1-6] that Ps is trapped in the more open parts of molecular crystals (e.g. amorphous regions, etc.), PAT studies of Ps trapping have not yet been used as a tool in the investigations of molecular crystal defects in the same way as positron trapping is used for metals. One reason for this is probably that very little information is available on vacancy-type defects in molecular crystals. In general, the Ps trapping method is probably also too sensitive compared to the degree of perfection of the presently available molecular crystals. Our results[18] indicate that very few ortho-Ps atoms are trapped before the annihilation takes place at a relative concentration of "holes" of roughly 10^{-7}, while all ortho-Ps atoms annihilate from a trapped state at a concentration of 10^{-4}. Ice is well suited for the study of Ps trapping because the relative concentration of Ps trapping defects in ice is so low ($\leq 10^{-7}$) that Ps annihilates from the non-trapped state at temperatures below -100°C. Our ice investigations seem to be the first detailed studies of defects in a molecular crystal carried out by the Ps trapping method.

From the viewpoint of solid state physics, a further aspect of our work is of importance. The non-trapped Ps-atom is in a Bloch function state in ice[19]. Apparently, Ps is the only atom that has been shown to be in a Bloch function state. Moreover, the angular correlation technique directly determines the numerical value of the Fourier transform of the para-Ps center-of-mass wave function. Such detailed information about wave functions does not seem not to be available in the case of electrons in metals and semiconductors, where Fermi surfaces and properties calculated from matrix elements between initial and final states (optical absorption, photoeffect, etc.) are chiefly measured[20]. In particular, the change in the para-Ps

wave function due to trapping in defects is easily measured. The trapping of ortho-Ps can be followed by use of the lifetime technique. Hence, the Ps state can be studied at two different times after Ps formation. Experimental evidence for Ps in a Bloch-function state has been found for quartz[21-26], H_2O- and D_2O-ice[19], MnF_2[26], MgF_2[26], NaF (-196°C)[27], and NaCl (-196°C)[27]. Apparently, no systematic search for delocalized Ps in crystals has been performed, but probably Ps annihilates from a Bloch function state in many other crystals of low defect concentration.

The present paper is part of an experimental series on positron annihilation in ice and related structures[18,19,28-32]. We attempt here to give a fairly complete discussion of the results obtained hitherto. Previously, ice has been studied several times by other PAT groups (see e.g. refs. 1 and 33). In fact, ice was and is one of the most studied crystals.

The experimental apparatus and the measurements are discussed in section 2. In section 3 a description of the results and the fairly complicated data analysis is given. The theory of annihilation from the Ps state and the influence of the thermal motion of the atoms on the Ps Bloch function are discussed in section 4. A general discussion of the Ps yield, the Ps Bloch function, the Ps trapping process, and the defects that trap Ps in ice is found in section 5, followed by some concluding remarks in section 6.

2. EXPERIMENTAL

For the angular correlation measurements, a standard linear-slit setup was used[1-6]. The detectors were NaI(Tl) cylinders, of about 39 cm in length and 5 cm in diameter. Two EMI9708 photomultiplier tubes faced each cylinder. One mm slits in 5 cm thick lead bars, placed in front of the detectors, covered a solid angle of 0.48 x 178 mrad, as seen from the sample. The pulse-handling electronics was a normal fast coincidence system with an effective coincidence resolving time of 82 nsec (full width at half maximum (fwhm) of coincidence counting rate as a function of time delay), and energy windows placed at the photopeak. A digital control system, similar to that described in ref. 34, automatically adjusted the angles (read from tape and measured by shift digitizers), and trans-

ferred angles and measured numbers to a teleprinter for output. The output on tape was further processed by a computer. Typically, the curves were measured in steps of roughly 0.2 mrad at the peaks, 0.4 mrad at normal parts, and 0.6 mrad at the larger-angle parts of the curves (see Figs. 1-3). The curves were measured in many scans of the angles in order to minimize the effects of drift in the system.

The samples (approx. 5 mm thick plates) were placed in a roughly 40 mm diameter, 10 mm high box. They were fixed with grease to the copper bottom of the box. The box was mounted on a thick copper plate, which was cooled by heat conduction to the cold finger of a liquid nitrogen cryostat. The desired temperatures were obtained by heating the sample by means of an electric heater controlled by a thermostat. Two thermocouples melted into the side of the samples measured the temperature. An external sources of about 20 mCi ^{22}NaCl was placed above the sample box. The positrons hit the sample through a 19 mm diameter Mylar window. The window also served as a collimator to prevent the positrons from directly hitting part of the box sides from where the annihilation photons could reach the detectors through the 2 mm shield slits placed close to the box. The sample box and source were mounted in an evacuated chamber ($\approx 10^{-2}$ mm Hg pressure). Below approximately -70°C the box was also evacuated. Above -70°C the box contained helium at atmospheric pressure to strongly reduce the sublimation of the ice samples. The angular resolution was determined by the slit widths (a triangular resolution curve of fwhm 0.48 mrad) and the smearing due to the uncertainties in the effective sample heights. The latter is caused by the penetration ($\approx$ 0.3 mm) of the positrons into the sample, and the fact that the sample was tilted somewhat in order that the annihilation photons should be emitted to the movable slit through the side of the sample for all angles. Roughly speaking, the resolution curve may be described by a Gaussian of fwhm $\approx$ 0.65 mrad. A more detailed discussion of the angular resolution curve will be given in subsection 5.7.

The lifetime spectrometer used was a conventional fast-slow coincidence system[3,18] with a time resolution characterized by a fwhm = 0.42 nsec. As source was used about 6 μCi of ^{22}NaCl sealed between two 1 mg/cm^2 nickel foils. The frac-

tion of positrons annihilating in the source and foils was estimated at 10%[35]. The source-sample sandwich was mounted in a cryostat and the temperature controlled as described in ref.32. Data were collected for each spectrum over periods of 2-5 days resulting in 6-17 x 10^5 counts in a spectrum.

Most of the pure ice single crystals were grown by G.Kvajić at Vincha, Belgrad. They were grown at a rate of 10^{-4} cm/sec. by a modified Bridgeman method using triple destilled water. They were zone-refined once and not grown under vacuum. Hence, an equilibrium concentration of air molecules (N_2, O_2, CO_2, Ar, etc.) was always present in the liquid phase. A few pure ice single crystals grown by J. Bilgram, ETH, Zürich, were also used[36].

Some of the crystals for the angular correlation measurements were oriented by X-ray diffraction by Bilgram. For the others, the c-axis was determined by polarized light and the a-axis by an etch pit technique similar to that of ref. 37. The crystals were cut on a lathe, and then ground with fine emery paper and polished with a soft cloth and silk. The accuracy of the orientations of the final samples was estimated to be better than 5°. All crystal treatments were carried out in a cold room at -18°. Lathe cutting of the crystals certainly introduces some defects in them, in particular dislocations[38]. However, these dislocations do not seem to be detected by positrons or Ps, as we found no measurable effect of different initial sample treatments. A similar conclusion was reached in ref. 18.

3. DATA ANALYSIS AND RESULTS

3.1. Measurements

In the present work we measured angular correlation curves for monocrystals of light and heavy ice for various crystal orientations and as a function of temperature from -182°C to the melting point, a total of about 50 curves. Some of the measured curves are shown in Figs. 1-3, in Figs. 2 and 3 with a broad component subtracted to show more clearly the narrow ($\sim$ 1 mrad) components. A few other curves have been published in refs. 12, 28, and 39. The clear general feature is that with increasing temperature the intensities of the narrow central peaks (at 0 mrad) and side peaks decrease followed by a simul-

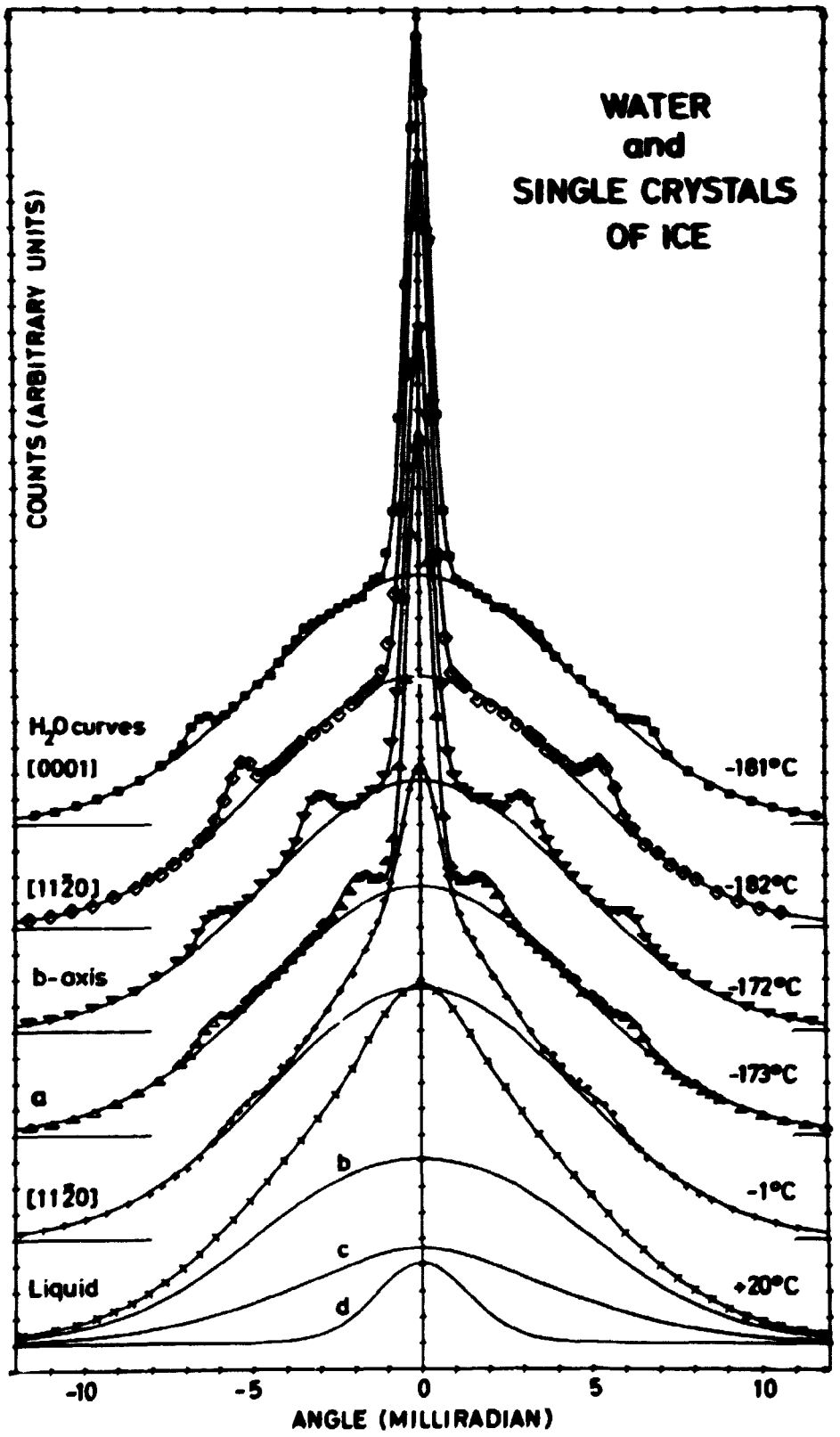

Fig. 1. The measured points and the fitting curves of the angular correction distributions in water and single crystals of ice. The z-directions are shown in Fig. 4. The z-direction of curve a is in the plane of the a- and c-axes and tilted 20.6° from the c-axis. Curves b, c, and d are the "free" positron, ortho-Ps pick-off, and para-Ps contributions to the water curve, respectively. The measured curves are normalized to equal area. The uncertainties are smaller than or equal to the size of the points.

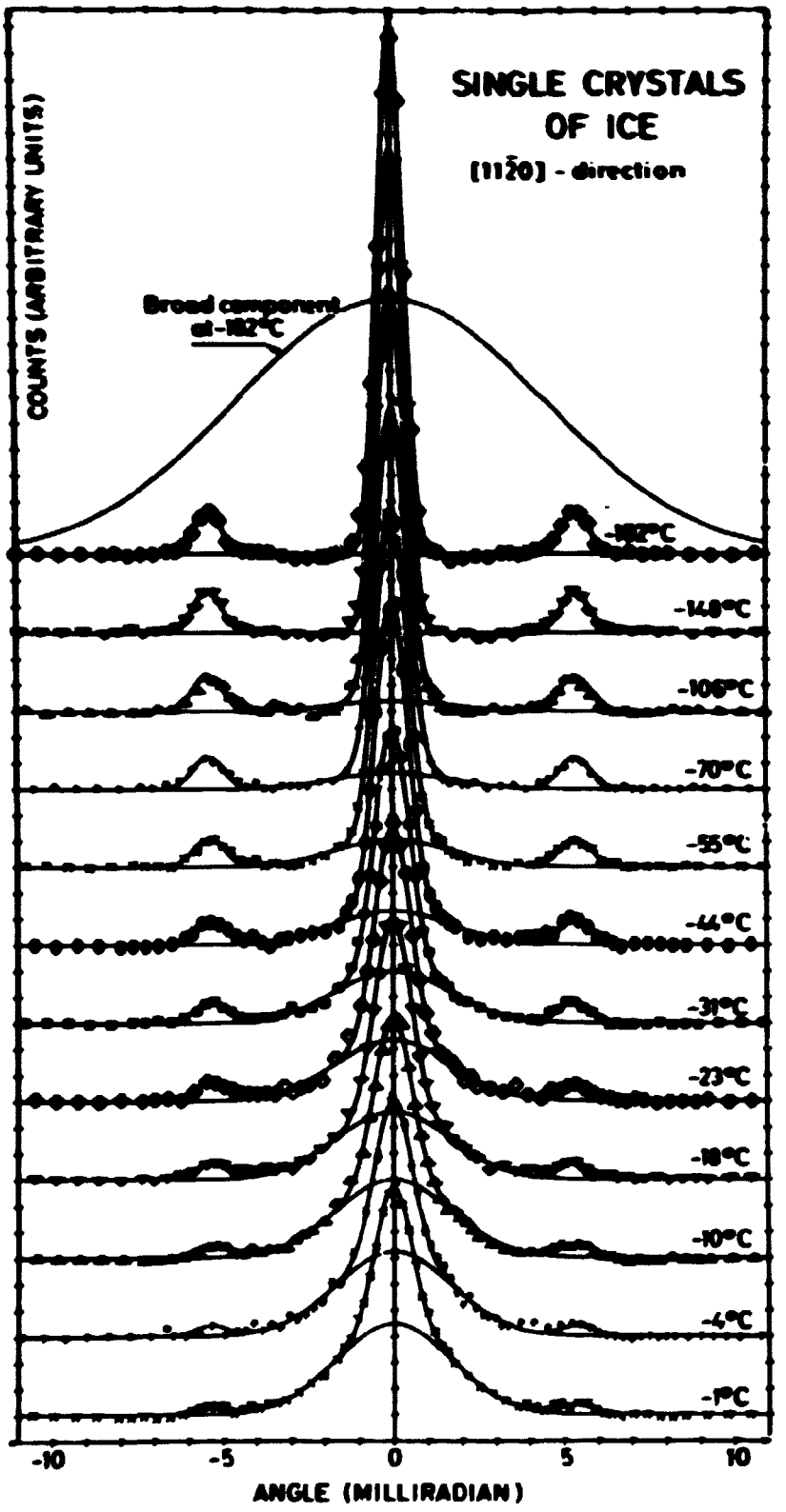

Fig. 2. The temperature dependence of the angular correlation curves for single crystals of H_2O-ice oriented along the a-axis. The measured points and the fitting curves are shown after the subtraction of the broad component from the normalized curves. Only the uncertainties greater than the size of the points are shown.

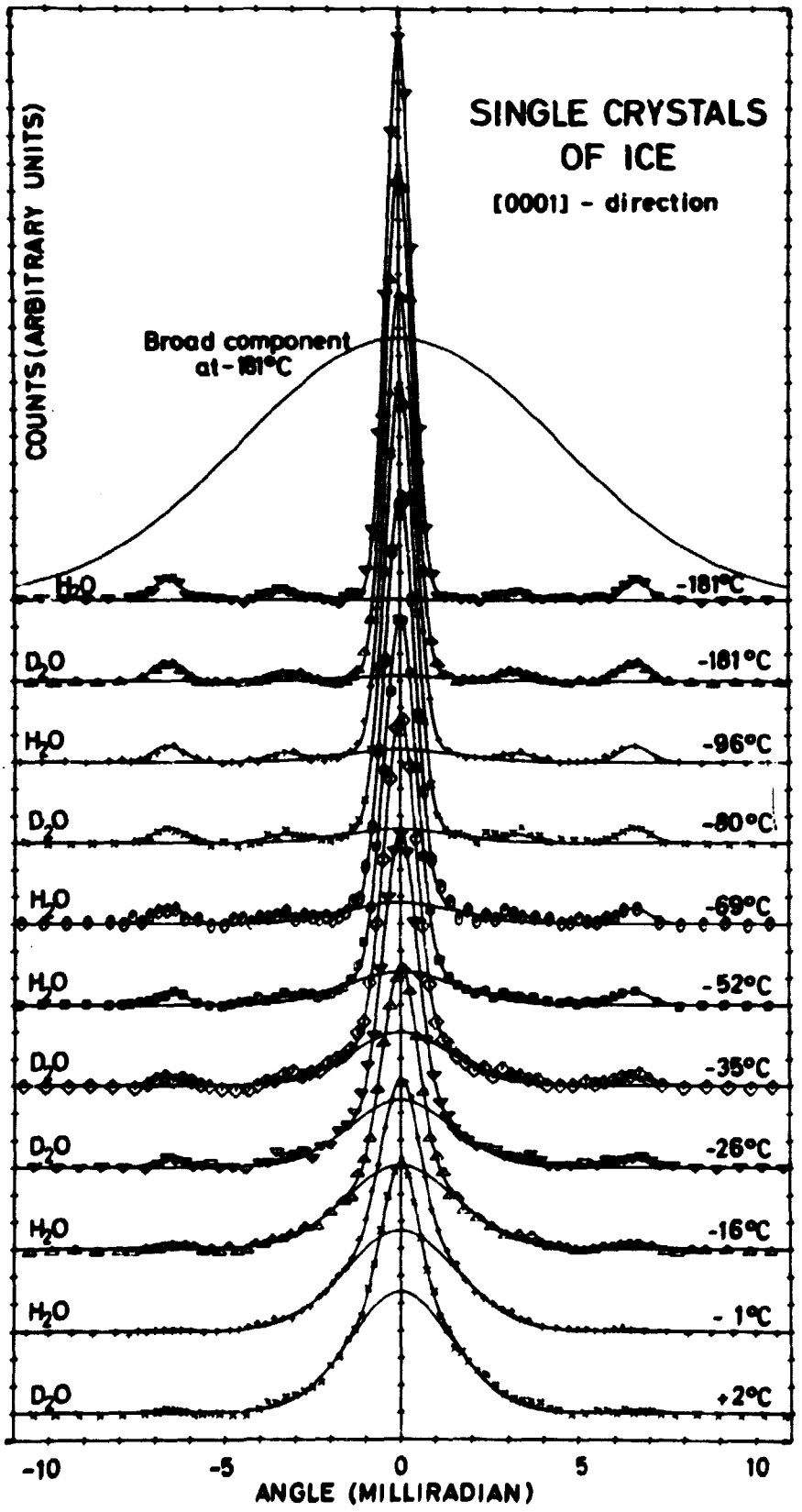

Fig. 3. The temperature dependence of the angular correlation curves for single crystals of H_2O- and D_2O-ice oriented along the c-axis. The measured points and the fitting curves are shown after the subtraction of the broad component from the normalized cruves. Only the uncertainties greater than the size of the points are shown.

taneous increase in intensity of a somewhat broader ($\sim$ 3.8 mrad) component (Figs. 2, 3). The crystal orientations relative to the reciprocal lattice points are shown in Fig. 4. To obtain quantitative information about these - and other - changes with temperature, we carried out a detailed analysis of the measured curves, which is outlined in sections 3.3 and 3.4. The results are shown in Figs. 5-7, and in tables 2 and 3.

We also remeasured some lifetime spectra for light ice at temperatures between -175°C and the melting point (previously published in ref. 18). This was done to try to answer the question whether the long (ortho-Ps) lifetime at higher temperatures is one single lifetime component or a sum of two (see section 5). Therefore, we used a relatively weak source to reduce the background and nickel foils around the source material to avoid longlived source-components. Finally, we collected as many counts as possible to get good statistics. The analysis of the spectra and their results are discussed in the following section 3.2.

3.2. Lifetime Spectra: Analysis and Results

The measured lifetime spectra were analyzed by means of the computer program Positronfit Extended[40]. A sum of three Gaussians was used to describe the time resolution curve in as much detail as possible. Their fwhm's and intensities were determined by a method similar to that described in ref. 35. These values were: 0.409 nsec, 54.4%; 0.517 nsec, 36.8%; 0.60 nsec, 8.8%.

A new result of the analysis was that, at the highest temperatures (-5°C), a longlived component (apart from the $\tau_3 \sim 1$ nsec and the two shorter components (τ_1, I_1 and τ_2, I_2) found in ref. 18) could be resolved with a lifetime of $\tau_4 = 1.7 \pm 0.4$ nsec. To take this component into account, all spectra were analyzed to extract four lifetime components, keeping $\tau_4 = 1.7$ nsec (four term, non-constrained analyses would only give meaningful results at the highest temperatures). This analysis gave an intensity I_4 that was close to 0.5% below -100°C, increased to about 1.7% at -40°C and then sharply increased to 5.1% at -5°C. The other three lifetime components could not be reliably separated for temperatures below -60°C. Above -60°C, τ_3 increased with temperature, I_3 being essentially constant = 51 $\pm$3%,

while the other components showed variations in agreement with our previous measurements[18]. The values obtained for τ_3, I_3, and I_4 at four temperatures at and above -60°C are given in table 1. Of course the question arises about the reliability

Table 1

The most important lifetime parameters above -60°C. In the analysis τ_4 was fixed at 1.7 nsec. The uncertainties are estimated standard deviations caused by the statistical scatter of the data.

Temperature (°C)	τ_3 (nsec)	I_3 (%)	I_4 (%)
-60	0.776 ± 0.015	48.2 ± 2.0	1.8 ± 0.2
-40	0.825 ± 0.039	53.0 ± 7.7	1.6 ± 0.5
-21	0.950 ± 0.029	51.3 ± 3.5	2.6 ± 0.6
-5	0.990 ± 0.018	50.5 ± 1.3	5.1 ± 0.6

of the results of such a four component analysis (even with one lifetime fixed). There seems to be no doubt, as strongly suggested in ref. 18, that more than 3 lifetime components are present at the higher temperatures, and analysis of computer simulated spectra has also excluded the τ_4 component as being an artifact of the analysis. Regarding the main longlived component (τ_3, I_3) one might suggest that it has contributions from one or more decay processes with only slightly different lifetimes (up to ~50% difference. τ_2 is about 0.4 nsec[18]). Clearly they could not be separated, but the uncertainty on I_3 would be rather large. This does not seem to be the case for the present spectra above -60°C (table 1). In this connection it is worth noticing that lifetime spectra for HF doped ice at low temperatures also contain longlived components associated with ortho-Ps trapping. In these spectra, however, the long lifetime part cannot in general be described by only one component (τ_3, I_3) with constant I_3, but must be a composite of at least two components, of which one has a constant lifetime (τ_3= 1.2 nsec) and the other one mixes with the shortlived components[31]. Hence, we believe the suggestion of the analysis of the present results, viz. that the resolved main longlived

component (τ_3, I_3) is essentially one single component with temperature. The constancy of I_3 (or $I_3 + I_4$ within uncertainty) is satisfactory, because it was presupposed in the analyses in ref. 18.

3.3. Analysis of the Angular Correlation Curves

The basic idea of the analyses of the angular correlation curves is that Ps is formed in ice, and that the narrow central peak and side peaks (Figs. 2-3) are the results of intrinsic para-Ps annihilation from a Bloch function state for the center-of-mass coordinate (see section 4). The middle-broad component of full width at half maximum roughly equal to 3.8 mrad, appearing at higher temperatures, results from intrinsic para-Ps annihilation of Ps-atoms trapped in a defect in the ice lattice. We are mainly interested in the temperature dependence of the Bloch function and in the Ps trapping in the defect. The main purpose of the analyses is therefore to extract from the curves the intensities and fwhm's of the narrow peaks and the middle-broad component. However, the analyses also serve as a fairly detailed test of the above-mentioned basic interpretation of the curves.

The counts at the top of the curves were typically 32000 (20000) at low (high) temperatures. Examples of curves with unusually small and large counting statistical uncertainties are the $-181^{\circ}C$ D_2O-curve in Fig. 3 (63000 at the top) and the $-4^{\circ}C$ curve in Fig. 2 (10500 at the top). The output tape from the angular correlation setup was first analyzed by means of the PAAC computer program. A random background of roughly 0.1% of the counts at the top was subtracted. Because of positron backscattering, etc., some annihilations took place in the walls of the sample-box. An empty box gave a curve well fitted by the three Gaussians with relative intensities (fwhm's): 1.9% (2.62 mrad), 61.1% (8.55 mrad) and 37.0% (22.62 mrad), and an absolute intensity of roughly 7.3% of the ice curve intensities. This curve was subtracted from all the ice curves. Because the number of annihilations on the sample-box wall might have changed when the sample was placed in the box, this correction could have introduced a small error in the curves. The PAAC output was the corrected angular correlation curves on cards, in a plot, and in a table.

The PAACFIT program was used for the computer analyses of the angular correlation curves. Without such a program, a detailed analysis of many curves is virtually impossible to perform. This program has been described in detail elsewhere[39]. It fits an angular correlation curve by means of central Gaussians and side-peak pairs of Gaussians. The fitting parameters are the intensities (i.e. the relative areas in %) and full widths at half maximum (fwhm) of the Gaussians and the symmetry angle of the curve. The side-peak positions are fixed in the analysis. Both positive and negative intensities can be used. The intensities and fwhm's of the Gaussians can be fixed in the analysis. Other possible contraints are to put linear combinations of intensities equal to zero. These constraints combined with the use of fixed fwhm's make possible an analysis of a curve in terms of other curves the parameters of which have been determined in other analyses. The program also finds the goodness of the fit, ϕ, calculated on the assumption that the model is ideal, in which case $\phi = 1 \pm 0.2$. Since our models are not ideal we have to accept greater ϕ-values. We obtained ϕ-values between 1.5 and 4 for good fits of our normal curves with 25000 counts at the top of the curves. The program has been used with good results in studies of Ps-chemistry problems[41] and of positron trapping in vacancies and voids in molybdenum[35]. We have also tested the program by analyzing computer-generated curves of shape close to that of the ice single crystal curves and with typical values of the scatter.

A more detailed discussion of a series of analysis of the a-axis (see Fig. 4) ice curves will illustrate some of the problems we encountered in the fitting procedures. At low temperatures, the curves consisted of a broad component, a narrow central component, and a side peak pair, while at higher temperatures a middle-broad component was found too. At first, we analysed nearly all the a-axis curves by means of three central Gaussians and one pair of side peak Gaussians. The side peak positions were calculated by use of the ice lattice parameters[42] (see Fig. 4 and subsection 4.3). The fit was good, but for many of the curves the values of the fitting parameters were not acceptable. For example, the fwhm's of the side peaks sometimes attained values of 5 to 10 mrad at some of the highest temperatures where the side peaks were rather small. For the a-axis

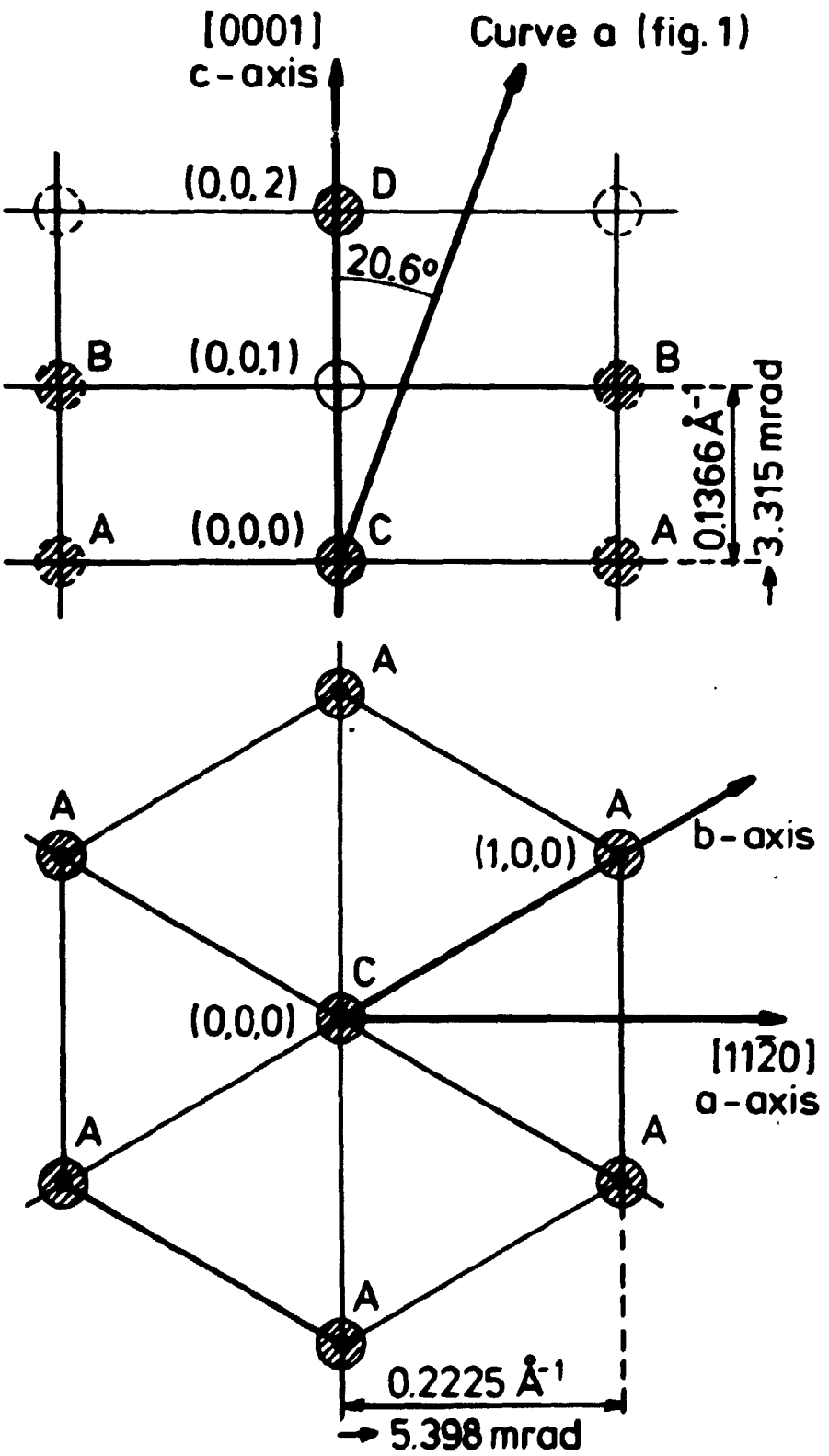

Fig. 4. The reciprocal lattice of ice. The hatched points contribute to the angular correlation curve due to intrinsic para-Ps annihilation. The diameter of the circles corresponds roughly to a width of 0.9 mrad (roughly the measured fwhm of the narrow peaks).

$-182^{o}C$ curve (see Fig. 1) the broad component was well fitted by two Gaussians (84.676% with fwhm = 10.394 mrad and -1.013% with fwhm = 5.870 mrad). A one-Gaussian fit of the broad component was rather poor and three Gaussians did not give a significantly smaller variance of the fit. For the other low temperature curves, the shape of the broad component was not significantly different from that of the $-182^{o}C$ curve.

We then analyzed the curves by use of four central Gaussians and a pair of side peak Gaussians. The shape of the broad component was fixed to the shape found at $-182^{o}C$ by use of fixed fwhm's and one linear-combination-of-intensities constraint. Again the parameters for some of the higher temperature curves were unacceptable. The reason for this was that the larger angle parts of the curves strongly influenced the intensity of the broad component, and hence the side peaks and middle-broad component were to some extent used to compensate a too small or a too large broad component at smaller angles.

From theory we expected that the broad component would be approximately independent of temperature except for a small correction of the intensity. This was found to be roughly in agreement with the results of the first analyses. To be able to fix the broad component intensity, I_B, we must know its temperature dependence. We assumed that para-Ps is either in a Bloch function state or in a trapped state. This assumption might be partly incorrect (see subsection 4.3). However, I_B varied very little with temperature and hence it did not depend much on the assumption used. We find

$$I_B = I_0 + I_b \lambda_{pb}/(\lambda_0 + \lambda_{pb}) + I_t \lambda_{pt}/(\lambda_0 + \lambda_{pt}) \qquad (1)$$

where I_0 is the broad component due to ortho-Ps and free positron annihilation, and the other two terms are the para-Ps pick-off contributions in the bulk and trapped states, respectively. Hence, $\lambda_0 = 8 \cdot 10^9$ sec^{-1} is the intrinsic para-Ps decay rate, and $\lambda_{pb}(\lambda_{pt})$ is the pick-off rates in the bulk (trapped) state. $I_b(I_t)$ is the total para-Ps intensity in the bulk (trapped) state. From lifetime results[18], we may assume that $\lambda_{pb} = 1.49 \cdot 10^9$ sec^{-1} and $\lambda_{pt} = 0.81 \cdot 10^9$ sec^{-1}. On assuming that the total probability of para-Ps formation, $I_b + I_t$, is independent of temperature (see section 5), we find from equation (1)

$$I_B(t) = I_B(-180^oC) - 0.065 \cdot I_t(t) \quad (2)$$

To calculate $I_B(t)$, we first used I_t-values extracted from the lifetime results assuming that the relative amounts of ortho-Ps and para-Ps trapping were equal at a given temperature (see section 5). However, the amount of para-Ps trapping is best determined by use of the angular correlation curves. Hence, in the following analyses we calculated $I_B(t)$ from the I_t-values extracted by the foregoing analysis. In the final analyses we used

$$I_B(t) = 83.66 - 1.26(1-C_a(t)/13.821) \quad (3)$$

where C_a was the central peak intensity of the a-axis curves. The shape of the broad component was always equal to that of the -182^oC curve (84.676% (10.394 mrad) and -1.013% (5.870 mrad)).

In the next, fixed-broad-component analysis nearly all parameters were acceptable, but some high temperature values were still too uncertain. We then also fixed the side peak fwhm's to (t in ^oC, fwhm in mrad).

$$fwhm(t) = 1.116 + 9.05 \cdot 10^{-4} \cdot t, \quad (4)$$

because this expression fitted well the side peak fwhm's determined in the fixed-broad-component analysis. The fwhm's of the middle-broad component at temperatures above -40^oC, where it was well defined, were then found to be very constant. We found fwhm = 3.94 $\pm$ 0.09 mrad from 11 curves.

In the final analysis of the a-axis curves we therefore also fixed the fwhm of the middle-broad component to be 3.94 mrad. This gave a goodness of the fits fairly close to the best values obtained in the analyses where all the parameters were free. The freely variable parameters came out of the analyses well defined.

The c-axis ([0001]) curves were treated in a similar way. At low temperatures, the curves were well fitted by two central Gaussians and two side peak pairs of Gaussians, which resulted in good fit of the broad component by one Gaussian of 83.66% with fwhm of 10.59 mrad. In the following analyses, we fixed

the broad component to this shape and to an intensity calculated by use of expression (3). Expression (4) was used to fix the side peak fwhm's. The inner side peak pair of low intensity was only well defined at low temperatures, where we found an average intensity of 0.559% and a ratio between the intensities of the outer and inner side peaks of 2.09. Hence, in the following analyses, we fixed the inner side peak pair intensity to be 1/2.09 times the intensity of the outer side peak as determined in the foregoing analysis. The side peak positions were determined by use of the lattice constants of ice[42] (see Figure 4 and subsection 4.3).

As in the a-axis analyses, the fwhm of the middle-broad component was then fixed to be the average value determined in an analysis where the above-mentioned constraints were used. For temperatures above -40%, we found fwhm = 3.70 $\pm$ 0.22 mrad for the H_2O-curves and fwhm = 3.42 $\pm$ 0.14 mrad for the D_2O-curves, while the average of all the curves was fwhm = 3.56 $\pm$ 0.23 mrad. Although the difference between the H_2O- and D_2O-values was not much larger than the uncertainty, we fixed the fwhm's of the H_2O- and D_2O-vurves to these two different values in the final annalysis. Such small fwhm differences introduced only very small changes into the freely variable fitting parameters determined in the analysis.

All the fitting curves shown in Figs. 2 and 3, and the a- and c-axis curves in Fig. 1, are the results of the final PAACFIT analyses (i.e. fixed broad-component shape and intensity, and fixed fwhm's of the side peaks and middle-broad components). In Fig. 1 are also shown the broad components. The low-temperature broad components and the middle-broad components are shown in Figs. 2 and 3. The intensity of the middle-broad component is shown in Fig. 5. The final fit fwhm's of the central peak are shown in Figs. 6 and 7. In table 2 are shown the values of the freely variable and some of the fixed, final fit parameters for a number of the curves.

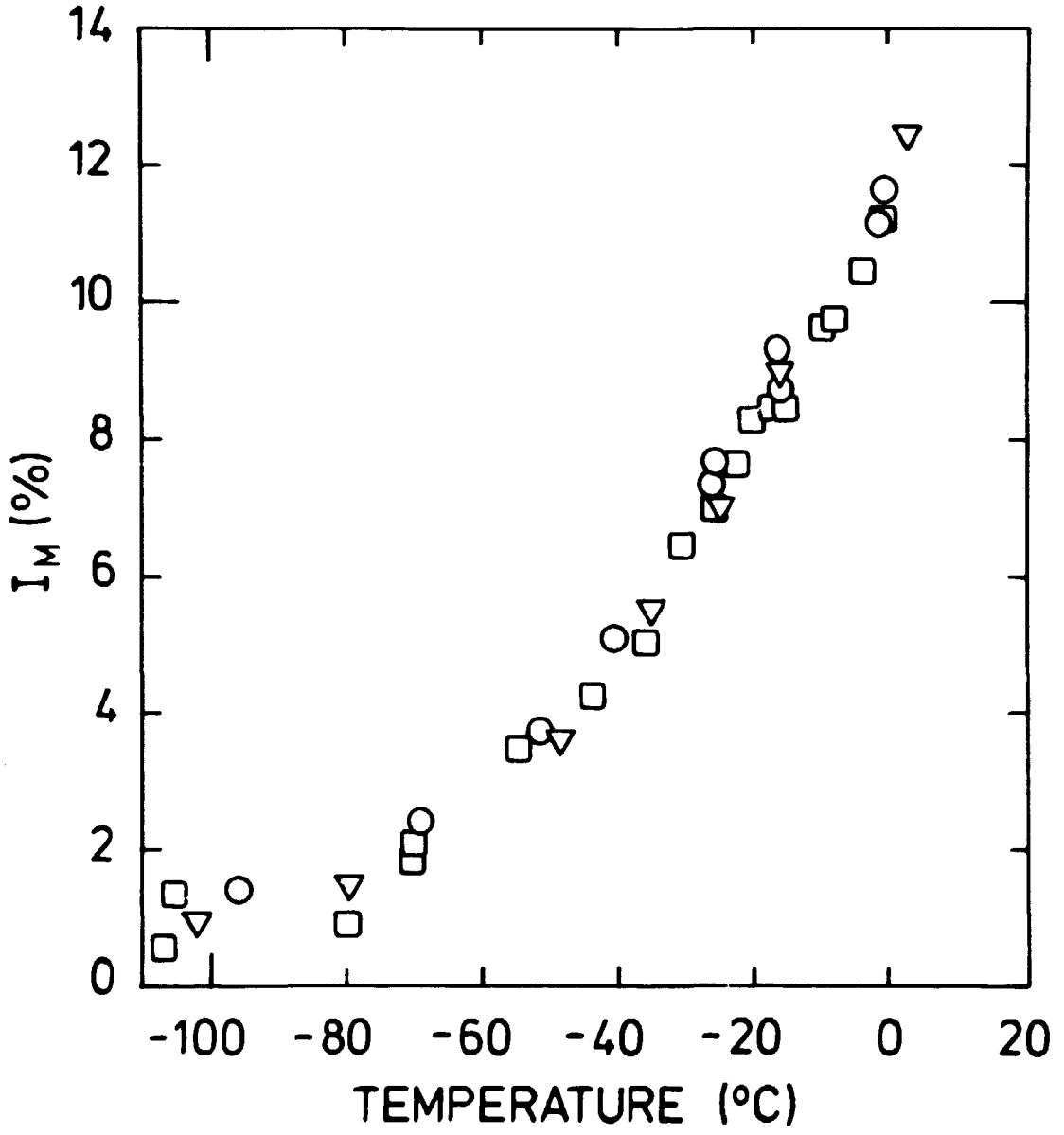

Fig. 5. The intensity of the middle-broad component (fwhm = 3.94, 3.70, and 3.42 mrad for the H_2O a-axis, H_2O c-axis, and D_2O c-axis, respectively) versus temperature. The squares and circles are for H_2O a- and c-axis crystals, respectively, and the triangles for D_2O c-axis crystals.

Table 2

The fitting parameters of several typical angular correlation curves. The side peak positions and the f-marked parameters were fixed in the fitting analysis. The reference curves are the chosen average curves at low temperature. The shapes of broad components are given in section 3.3. c(s) refer to central (side) peak intensities and subscript a, c, and b to a-, c-, and b-axis orientations, respectively.

a-axis curves	C_a (%)	S_a (%)		Middle-broad (%)	Broad (%)	Central fwhm (mrad)	Side peak position (mrad)		Side peak fwhm (mrad)
Reference	13.821	2.517		0.0	83.66				
-182°C	13.813	2.517		0.007	83.663f	0.849	5.398		0.950f
- 31°C	8.903	1.395		6.460	83.243f	1.169	5.375		1.089f
- 1°C	5.223	0.666		11.203	82.909f	1.224	5.370		1.115f
c-axis curves	C_c (%)	S_{c1} (%)	S_{c2} (%)	Middle-broad (%)	Broad (%)	Central fwhm (mrad)	1. Side peak position (mrad)	2. Side peak position (mrad)	Side peak fwhm (mrad)
Reference	14.612	0.559	1.169	0.0	83.66				
H_2O, -181°C	14.559	0.559f	1.167	0.054	83.660f	0.861	3.315	6.630	0.950f
D_2O, - 26°C	9.082	0.235f	0.552	6.940	83.191f	1.116	3.299	6.598	1.093f
H_2O, - 1°C	5.742	0.088f	0.120	11.142	82.908f	1.263	3.295	6.590	1.115f
D_2O, + 2°C	4.530	0.070f	0.145	12.388	82.867f	1.161	3.295	6.590	1.117f
b-axis curve	C_b	S_{b1}	S_{b2}	Middle-broad (%)	Broad (%)	Central fwhm (mrad)	1. Side peak position (mrad)	2. Side peak position (mrad)	Side peak fwhm (mrad)
-172°C	12.562f	2.517f	1.259f	0.0f	83.66f	0.876f	3.113	6.226	0.950f

3.4. Reciprocal Lattice Point Contributions

The narrow peak intensities measured by a linear-slit setup are due to discrete contributions to the angular correlation curves situated at the reciprocal lattice points (see subsection 4.3). The reciprocal lattice points, which significantly contribute to the narrow peaks for ice, are shown hatched in Fig. 4 (see below for a more detailed discussion). We denote the contributions from the points of the (1, 0, 0) type by A, of the (1, 0, $\pm$1) type by B, of the (0, 0, 0) point by C, and of the (0, 0, $\pm$2) points by D. These contributions can be calculated from the following equations:

$$4A + 8B = S_a \tag{5}$$

$$2A + 4B + C + 2D = C_a \tag{6}$$

$$12B = S_{c1} \tag{7}$$

$$2D = S_{c2} \tag{8}$$

$$6A + C = C_c \tag{9}$$

where C_a(C_c) is the a-axis (c-axis) central peak intensity, while S_a, S_{c1} and S_{c2} are the a-axis, c-axis inner and c-axis outer total side peak intensities, respectively.

The A- and C-values were extracted from the a-axis results in the following way. At first, B and D were calculated by use of the S_{c2}-values on a smooth curve through the measured S_{c2}-points versus temperature and by putting $S_{c1} = S_{c2}/2.09$. These B- and D-values were then used to calculate A and C from equations (5) and (6). The relative A- and C-values are shown in Fig. 6, where 100% corresponds to A = 0.536% and C = 11.393%, respectively.

The D-values were calculated from the measured S_{c2}-values. We also calculated C from the measured C_c-values (equations (9) and (5)) by use of the S_a-values on a smooth curve through the measured S_a-values versus temperature and the B-values determined as discussed above. The relative C- and D-values are shown in Fig. 7, where 100% corresponds to C = 11.393% and D = 0.585%, respectively. The low temperature value of B is 0.0446%

The line through the C-points in Fig. 7 is the same line as shown in Fig. 6. Apart from the $+2^{\circ}C$ point, the C-values for D_2O (m.p. = $3.8^{\circ}C$) are shifted roughly $3.8^{\circ}C$ with respect to the H_2O-values. (There were no a-axis D_2O-samples). The uncertainties shown in Figs. 6 and 7 were calculated from the measured intensity uncertainties as estimated in the PAACFIT-analyses.

We also measured several b-axis curves. The b-axis is directed along a unit-cell vector in the reciprocal lattice and perpendicular to the c-axis (see Fig. 4). In Fig. 1 is shown a comparison between the measured points and a b-axis curve calculated by use of the A, B, C, and D values (see table 2) and a broad component of the a-axis shape. Only the total area of the curve was free to vary in the fitting. The fact that the fit is good strongly indicates that the used interpretation of the a- and c-axis curves is correct.

The curve denoted by a in Fig. 1 was measured in order to check whether the contributions from the (0, 0, $\pm$1) points were really zero, as we had assumed above and as was expected from the theory (see subsection 5.4). The curve through the measured points was calculated by means of the same model as used above. Hence, the four side peak positions were derived by use of the angle 20.6° with the c-axis (see Fig. 4), and the usual fwhm's, the A-B-C- and D-values, and the c-axis broad component were used. Except for a small manual adjustment of the angle with the c-axis, only the total area was free to vary in the fitting of the curve to the measured points. A curve where all the S_{c1} intensity was placed at the (0, 0, $\pm$1) points did not fit the measured points as well as the curve shown in Fig. 1. However, the difference between the two fitting curves was fairly small owing to the small intensity of the measured c-axis inner side peak pair. The contributions A to D will be discussed in more detail in subsection 5.4 (see table 3).

The liquid ice (water) curve and the three components shown in Fig. 1 will be discussed in ref. 43.

As the PAACFIT-analyses discussed above were fairly complicated, and because such detailed analyses have not been reported before except for the somewhat different analyses in ref. 35, it is worth considering some general aspects of the fitting procedure here. The main problem is not just to fit the

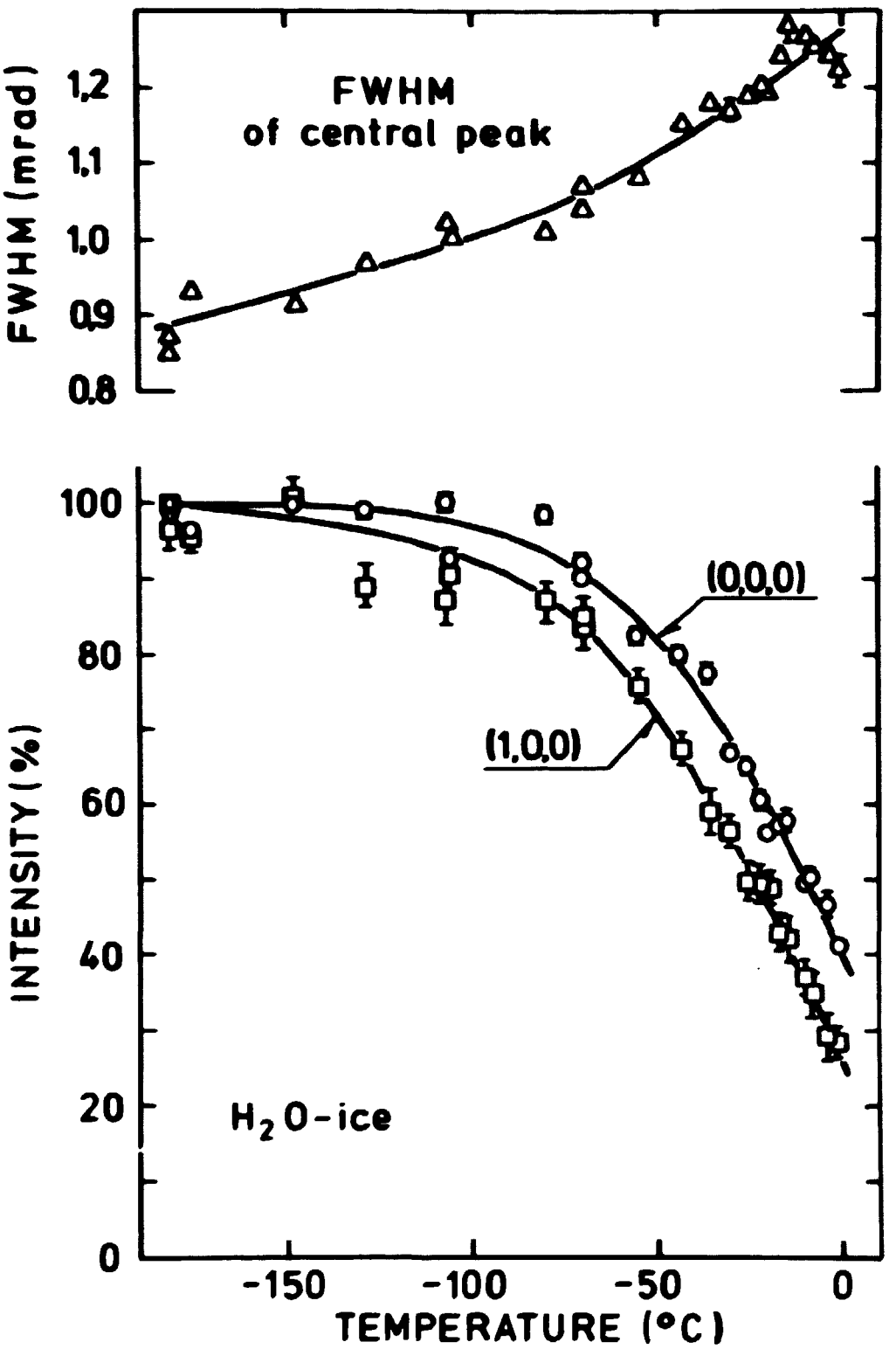

Fig. 6. The temperature dependence of the full widths at half maximum (fwhm) of the central peak and the relative intensities of the (0,0,0) (C) and (1,0,0) (A) type contributions to the narrow peaks for H_2O-ice, as derived from the c-axis angular correlation curves. The lines are handfits and the uncertainties are the computer estimates. 1000 corresponds to absolute intensities of 0.5360 for A and 11.3930 for C.

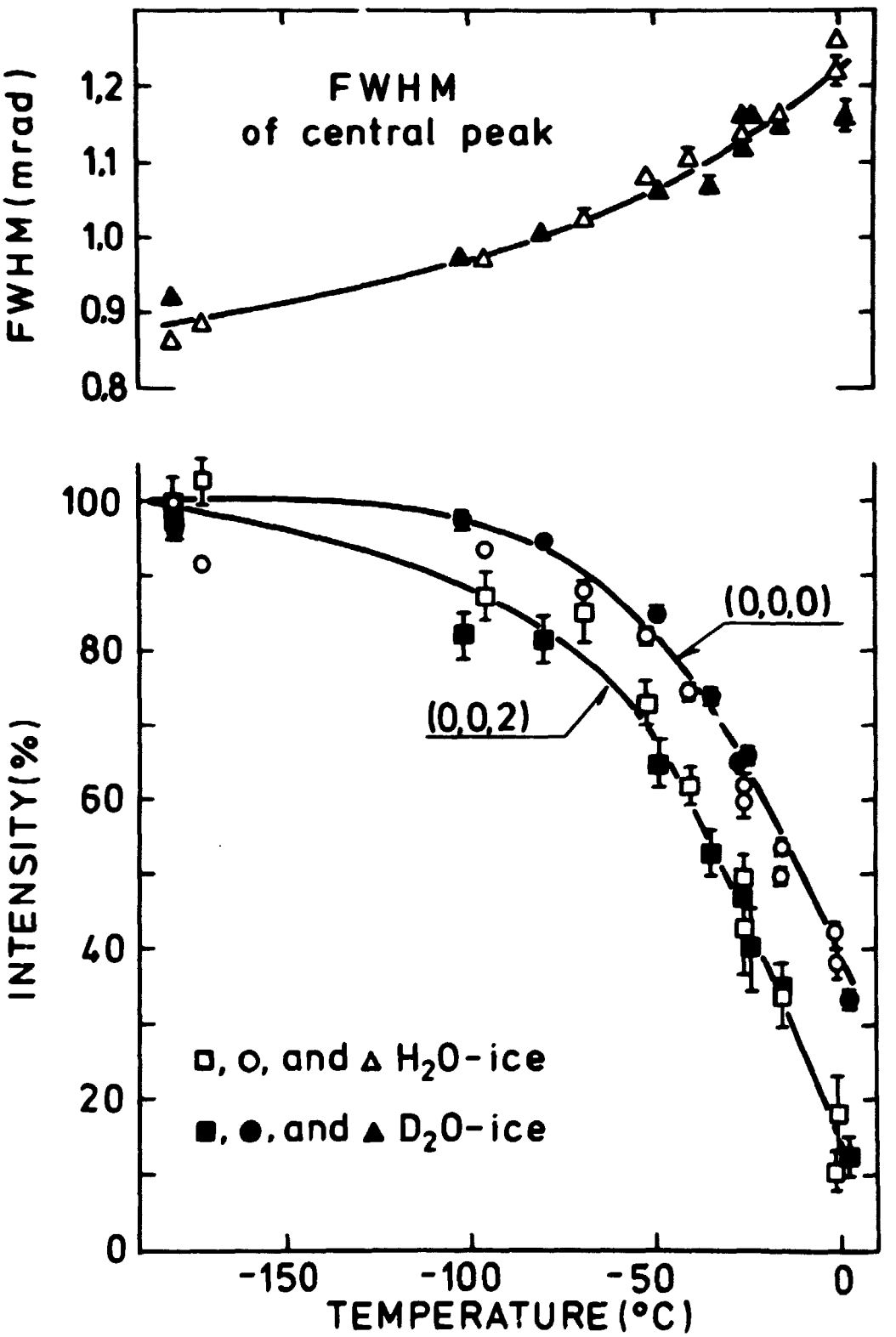

Fig. 7. The temperature dependence of the full widths at half maximum (fwhm) of the central peak and the relative intensities of the (0,0,0) (C) and (0,0,±2) (D) contributions to the narrow peaks for H_2O- and D_2O-ice as derived from the c-axis angular correlation curves. The lines are hand-fits and the uncertainties are computer estimates. 100% corresponds to absolute intensities of 9.585% for D and 11.393% for C.

curves well, but rather to fit the curves in such a way that well-defined fitting parameters can be unambiguously correlated to the various annihilation processes. There are several advantages of using such complicated analyses of the curves. First, it is virtually the only way to treat many curves in detail. Second, it is possible to extract more detailed information from the curves than in a manual treatment. Third, we obtain a well-fitting mathematical expression for each curve, which strongly facilitates the comparison of different curves and the presentation of many curves.

The use of constraints in the analyses is very important in this connection. It is perhaps appropriate here to emphasize that the main effect of the constraints used in the analyses is a reduction in the uncertainties of the extracted parameters. The constraints also make possible a reasonable analysis of a few of the curves that would otherwise be difficult to analyse (e.g. some of the high temperature curves). The important small effects extracted by the analyses (e.g. the difference between the H_2O- and D_2O-intensities in Fig. 7 and the small temperature dependence of the broad components) were qualitatively seen in the first non-constrained analyses too. A reasonable use of constraints makes possible a more quantitative discussion of these effects. Actually, before used the PAACFIT-program we processed some of the curves manually and obtained qualitatively the same results as in the later computer analyses (see the manually processed curves in Fig. 3 in ref. 28).

4. THEORY

4.1. General Remarks

To provide the basis for a detailed discussion of the experimental results in section 5, we shall in this section formulate and discuss the theory of the Ps state and the annihilation of Ps in solids. Since the discussion will be fairly general, several of the formulas derived will be valid for liquids too. In particular, we shall derive two new exchange terms in the 2-γ Ps annihilation probability, and discuss the influence of phonons on the intrinsic 2-γ annihilation from a Ps Bloch function state and the linear combination of a localized and a delocalized Ps wave function.

According to the spur reaction model of Ps formation[44-48], Ps is formed by a reaction between an excess electron and the positron in the terminal positron spur, which is the group of reactive intermediates (positron, excess electrons, positive ions, etc.) created when the positron loses the last 50-200 eV of its kinetic energy. Ps formation must compete with electron-ion recombination, with any electron or positron reactions with solvent molecules and scavengers, and with electron and positron diffusion out of the spur. Other processes, e.g. particle solvation in liquids and particle trapping in defects in solids, may also influence the Ps yield. The model indicates a strong correlation between the Ps formation probability and the electron-spur properties studied in radiation chemistry. Because effects that are very specific to the spur model, have recently been found[47,48], we believe that this model (and not the older, Ore model) correctly explains the Ps formation process. The positron spur in ice will be further discussed in section 5.

The main thermalization of the positron to an energy of about 200 eV is very fast ($\lesssim$ 0.1 psec), while the spur process of Ps formation probably takes 0.5-5 psec (a rough estimate). These times are short compared to the para-Ps (ortho-Ps) lifetime of roughly 120 psec (700 psec) in ice. Information on the Ps and positron states at annihilation is obtained by an angular correlation measurement. Lifetime measurements also give information about the fate of the positron and Ps during their lifetime. As we shall see in section 5, the great problems in the interpretation of the ice results are a) what is the Ps state at the formation and b) how does the Ps state vary with time in the interval between its formation and the annihilation. However, before we discuss the Ps state in detail we shall describe some new theoretical formulas for the annihilation probability expressed in terms of the wave function for the system.

4.2. Annihilation Probability

In 1967 one of us (O.E.M.)[49] derived from quantum electrodynamices, in a non-relativistic approximation, the following expression for the probability per unit time for annihilation into two photons, of which one is emitted into the space angle $d\Omega$, and for which the sum of the wave vectors $\bar{k} = \bar{k}_1 + \bar{k}_2$ is

within $d\bar{k}$

$$dw = \frac{r_o^2}{(2\pi)^3} d\bar{k}d\Omega \sum_{j=1}^{n} \sum_{\sigma_1} \int d\bar{r}_1 \ldots \sum_{\sigma_{j-1}} \int d\bar{r}_{j-1} \sum_{\sigma_{j+1}} \int d\bar{r}_{j+1} \ldots \sum_{\sigma_n} \int d\bar{r}_n$$

$$\left| \sum_{\sigma_j} \sum_{\sigma_p} \int d\bar{r}_j \; \varepsilon_{\sigma_p \sigma_j} e^{-i\bar{k}\cdot\bar{r}_j} \psi(\bar{r}_1\sigma_1, \ldots, \bar{r}_j\sigma_j, \ldots, \bar{r}_n\sigma_n, \bar{r}_j\sigma_p) \right|^2 \tag{10}$$

where $\psi(\bar{r}_1\sigma_1, \ldots, \bar{r}_n\sigma_n, \bar{r}_p\sigma_p)$ is the initial-state, non-relativistic Schrødinger wave function of a system of n electrons (variables $\bar{x}_j = \bar{r}_j\sigma_j$) and one positron ($\bar{x}_p = \bar{r}_p\sigma_p$). We use units where $\hbar = c = 1$. $r_o = \alpha/m$, where α is the fine structure constant and m the electron mass. $\varepsilon_{11} = \varepsilon_{22} = 0$ and $\varepsilon_{12} = -\varepsilon_{21} = 1$. In the derivation of (10) we first calculated the probability of transition from the initial state to a certain final state of the remaining electrons under the emission of two photons with quantum numbers $\bar{k}_1, \bar{e}_1$ and $\bar{k}_2, \bar{e}_2$ ($\bar{e}_1$ and $\bar{e}_2$ are the photon polarization vectors). We then summed all the probabilities for transition to any possible final electron state and to the possible states of photon polarizations. At last we transformed from the variables $\bar{k}_1$, $\bar{k}_2$ to $\bar{k}_1$, $\bar{k}$, and used the deltafunction, which ensures energy conservation, to integrate over $|\bar{k}_1|$ using polar coordinates for $\bar{k}_1$ (i.e. $d\bar{k}_1 = |\bar{k}_1|^2 d\Omega d|\bar{k}_1|$). This explains the particular probability given by (10). Expression (10) can be reduced somewhat by use of the antisymmetry in the electron coordinates. However, in its present, "symmetric" form it can also be used if the antisymmetry is disregarded (see below). Clearly, dw depends only on the initial wave function, and it is independent of the space angle Ω. The annihilation probability is determined by a) the density of electrons at the positron (since $\bar{r}_p = \bar{r}_j$ in (1)), b) the Fourier transform with respect to the coordinates $\bar{r}_j$ and $\bar{r}_p (\bar{r}_p = \bar{r}_j)$, and c) the fact that the electron spin direction must be opposite to that of the positron (assured by $\varepsilon_{\sigma_p\sigma_j}$).

The derivation in ref. 49 is not complete partly because some of the approximations used in the calculations introduced errors that could not be estimated. To the best of our know-

ledge, there is no complete and thorough derivation of the 2-γ annihilation probability for a many-electron positron system in the literature, and expression (10) has only been published in ref. 49. Chang Lee[50] used an infinite number of Foldy-Wouthuisen transformations for a non-relativistic derivation of a formula for this annihilation probability in terms of the initial and final wave functions. His calculations are very complicated, and frequently orders-of-magnitude estimations are used. However, Chang Lee's work is perhaps the most complete derivation available. A Fermi sea type of calculation (i.e. no external field present), which includes some relativistic corrections, is found in ref. 51.

Very recently we derived expression (10) by use of Chang Lee's final expression ((49) and (50) in ref. 50, we could not get the correct constant factor $r_o^2/(2\pi)^3$, perhaps we misunderstood Chang Lee's notation). We used the non-relativistic approximation and summed over all possible final states using (46) in ref. 50. Hence, provided we correctly understand Chang Lee's notation, etc., (there are two misprints in (49)) expression (10) is in agreement with Chang Lee's work. It also gives the correct formulas for well-known simple cases (e.g. the para-Ps lifetime, the lifetime expression in ref. 52, and the free and independent particle cases). The formulas used in Fermi sea work (see e.g. ref. 53) seem to differ from (10) by the additional use of the adiabatic hypothesis on the Coulomb potential between the particles. Hence, expression (10) is probably correct. We strongly emphasize that we have not performed a completely satisfactory derivation, nor a complete check of the derivation of others for this expression. Such a derivation (or check) would certainly be a very valuable contribution to positron annihilation studies.

Recently one of us (O.E.M.) continued the derivations[54]. In a fairly good approximation (see below) we may assume that the state of a system consisting of a Ps atom and n-1 electrons is described by the wave function

$$\psi = c_1 \, A \, \{\psi_p(\bar{x}_1, \bar{x}_p) \, \psi_1(\bar{x}_2, \ldots, \bar{x}_n)\} \, , \qquad (11)$$

where c_1 is a normalization constant ($c_1 = n^{\frac{1}{2}}$, if the Ps-electron does not overlap the other electrons), and A is the anti-

symmetry operator. $\psi_p(\bar{x}_1, \bar{x}_p)$ is the Ps wave function and $\psi_1(\bar{x}_2, \ldots, \bar{x}_n)$ is the antisymmetric wave function for the n-1 electrons. This wave function is substituted into (10). We shall not discuss the straightforward, but fairly elaborate calculations here. The following 2-γ annihilation probability, defined as for expression (10), was derived.

$$dw = \frac{r_o^2}{(2\pi)^3}\, d\bar{k}d\Omega\, \frac{|c_1|^2}{n} \Big[\Big| \sum_{\sigma_1} \int d\bar{r}_1 \sum_{\sigma_p} \varepsilon_{\sigma_p\sigma_1} e^{-i\bar{k}\cdot\bar{r}_1}\, \psi_P(\bar{r}_1\sigma_1, \bar{r}_1\sigma_p) \Big|^2$$

$$+ (n-1) \sum_{\sigma_1} \int d\bar{r}_1 \ldots \sum_{\sigma_{n-1}} \int d\bar{r}_{n-1} \qquad (12)$$

$$\Big| \sum_{\sigma_n} \int d\bar{r}_n \sum_{\sigma_p} \varepsilon_{\sigma_p\sigma_n}\, e^{-i\bar{k}\cdot\bar{r}_n}\, \psi_p(\bar{r}_1\sigma_1, \bar{r}_n\sigma_p)\psi_1(\bar{r}_2\sigma_2, \ldots, \bar{r}_n\sigma_n) \Big|^2$$

$$-(n-1) \sum_{\sigma_1} \int d\bar{r}_1 \ldots \sum_{\sigma_n} \int d\bar{r}_n \sum_{\sigma_n'} \int d\bar{r}_n' \sum_{\sigma_p} \sum_{\sigma_p'} \varepsilon_{\sigma_p\sigma_n}\, \varepsilon_{\sigma_p'\sigma_n'}$$

$$\Big(\Big\{ e^{i\bar{k}\cdot(\bar{r}_n - \bar{r}_n')}\, \psi_p^*(\bar{r}_1\sigma_1, \bar{r}_n\sigma_p)\psi_1^*(\bar{r}_2\sigma_2, \ldots, \bar{r}_n\sigma_n)\psi_p(\bar{r}_n'\sigma_n', \bar{r}_n'\sigma_p')$$

$$\psi_1(\bar{r}_2\sigma_2, \ldots, \bar{r}_{n-1}\sigma_{n-1}, \bar{r}_1\sigma_1) \Big\} + \Big\{ --- \Big\}^* \Big)$$

$$-(n-1)(n-2) \sum_{\sigma_1} \int d\bar{r}_1 \ldots \sum_{\sigma_n} \int d\bar{r}_n \sum_{\sigma_n'} \int d\bar{r}_n' \sum_{\sigma_p} \sum_{\sigma_p'} \varepsilon_{\sigma_p\sigma_n}\, \varepsilon_{\sigma_p'\sigma_n'}$$

$$e^{i\bar{k}\cdot(\bar{r}_n - \bar{r}_n')}\, \psi_p^*(\bar{r}_1\sigma_1, \bar{r}_n\sigma_p)\psi_1^*(\bar{r}_2\sigma_2, \ldots, \bar{r}_{n-1}\sigma_{n-1}, \bar{r}_n\sigma_n)$$

$$\psi_p(\bar{r}_{n-1}\sigma_{n-1}, \bar{r}_n'\sigma_p')\ \psi_1(\bar{r}_2\sigma_2, \ldots, \bar{r}_{n-2}\sigma_{n-2}, \bar{r}_1\sigma_1, \bar{r}_n'\sigma_n') \Big]$$

Complex conjugation is indicated by *. Hence, $\{---\}^*$ denotes the complex conjugate of the of the term in the $\{---\}$ brackets.

We then assumed that

$$\psi_p(\bar{x}_1,\bar{x}_p) = \psi_2(\bar{r}_1,\bar{r}_p)\ \psi_s(\sigma_1,\sigma_p)\ ,$$

where $\psi_s(\sigma_1,\sigma_p)$ was either the para-Ps or one of the three ortho-Ps spin wave functions[1]. Similarly, we assumed that $\psi_1(\bar{x}_2, \ldots, \bar{x}_n) = \psi_3(\bar{r}_2,\ldots, \bar{r}_n)\psi_4(\sigma_2,\ldots,\sigma_n)$, and that the state of the n-1 spins could be described by a uniform ensemble (i.e. the equal probability and random phase assumption).

This calculation resulted in the "spin-averaged" 2-γ annihilation probability defined as for expression (10)

$$dw = \frac{r_o^2}{(2\pi)^3}\, d\bar{k}\, d\Omega\, \frac{|c_1|^2}{n}\Big[\Big\{2\Big|\int d\bar{r}_1\, e^{-i\bar{k}\cdot\bar{r}_1}\ \psi_2(\bar{r}_1,\bar{r}_1)\Big|^2\Big\}_{para}$$

$$+\frac{n-1}{2}\int d\bar{r}_1\ldots\int d\bar{r}_{n-1}\ \Big|\int d\bar{r}_n e^{-i\bar{k}\cdot\bar{r}_n}\ \psi_2(\bar{r}_1,\bar{r}_n)\psi_3(\bar{r}_2,\ldots,\bar{r}_n)\Big|^2$$

$$-\Big\{(n-1)\int d\bar{r}_1\ldots\int d\bar{r}_n\int d\bar{r}'_n\ \Big(\Big\{e^{i\bar{k}\cdot(\bar{r}_n-\bar{r}'_n)}\ \psi_2^*(\bar{r}_1,\bar{r}_n)\psi_3^*(\bar{r}_2,\ldots,\bar{r}_n)$$

$$\psi_2(\bar{r}'_n,\bar{r}'_n)\ \psi_3(\bar{r}_2,\ldots,\bar{r}_{n-1},\bar{r}_1)\Big\} + \Big\{---\Big\}^*\Big)\Big\}_{para} \qquad (13)$$

$$-\frac{(n-1)(n-2)}{4}\int d\bar{r}_1\ldots\int d\bar{r}_n\int d\bar{r}'_n\ e^{i\bar{k}\cdot(\bar{r}_n-\bar{r}'_n)}\ \psi_2^*(\bar{r}_1,\bar{r}_n)$$

$$\psi_3^*(\bar{r}_2,\ldots,\bar{r}_{n-1},\bar{r}_n)\psi_2(\bar{r}_{n-1},\bar{r}'_n)\ \psi_3(\bar{r}_2,\ldots,\bar{r}_{n-2},\bar{r}_1,\bar{r}'_n)\ \Big]\ ,$$

where the supscript para indicates that the term only differs from zero if $\psi_s(\sigma_1,\sigma_p)$ is equal to the para-Ps spin function. The standard linear-slit angular correlation setup determines in a good approximation the distribution of the z-component of $\bar{k}$, i.e. the distribution we obtain by integrating over k_x, k_y, and Ω in (12) and (13).

The total annihilation probability (i.e. the reciprocal lifetime) is obtained by an integration over $\bar{k}$ and Ω. Since

$$\int d\bar{k}\ e^{i\bar{k}\cdot(\bar{r}_n-\bar{r}'_n)} = (2\pi)^3\,\delta(\bar{r}_n-\bar{r}'_n)$$

we find

$$w = 2\pi r_o^2 \frac{|c_1|^2}{n} \left[\left\{ 2 \int d\bar{r}_1 |\psi_2(\bar{r}_1,\bar{r}_1)|^2 \right\}_{para} \right.$$

$$+ \frac{n-1}{2} \int d\bar{r}_1 \ldots \int d\bar{r}_n |\psi_2(\bar{r}_1,\bar{r}_n)|^2 |\psi_3(\bar{r}_2,\ldots,\bar{r}_n)|^2$$

$$- \left\{ (n-1) \int d\bar{r}_1 \ldots \int d\bar{r}_n \left(\left\{ \psi_2^*(\bar{r}_1,\bar{r}_n)\, \psi_3^*(\bar{r}_2,\ldots,\bar{r}_n) \right. \right. \right. \qquad (14)$$

$$\left. \psi_2(\bar{r}_n,\bar{r}_n)\psi_3(\bar{r}_2,\ldots,\bar{r}_{n-1},\bar{r}_1) \right\} + \left\{ \text{---}^* \right) \Big\}_{para}$$

$$\left. - \frac{(n-1)(n-2)}{4} \int d\bar{r}_1 \ldots \int d\bar{r}_n\, \psi_2^*(\bar{r}_1,\bar{r}_n)\, \psi_3^*(\bar{r}_2,\ldots,\bar{r}_{n-1},\bar{r}_n) \right.$$

$$\left. \psi_2(\bar{r}_{n-1},\bar{r}_n)\psi_3(\bar{r}_2,\ldots,\bar{r}_{n-2},\bar{r}_1,\bar{r}_n) \right]$$

The four terms in expressions (12), (13), and (14) may be denoted intrinsic, pick-off, intrinsic-pick-off-exchange, and pick-off-exchange terms, respectively. Use of the wave function (11) without the antisymmetry operator would only give the two first terms in (12), (13), and (14). Correspondingly, the two exchange terms are zero if we use the approximation that the Ps-electron does not overlap the electrons of the many-electron system. To our knowledge, the last two, exchange terms have not been discussed before.

Of course, expression (11) is only an approximation of the wave function in condensed matter, and the more the two particles in Ps overlap the other electrons, the worse the approximation. On the other hand, expression (11) seems to be the best of possible approximations in which Ps can be associated with a wave function of its own. In a higher approximation the total wave function would no longer be separable as given in (11). One way of calculating the wave function would be to calculate ψ_1 taking into account the presence of Ps (including its influence on the atomic positions, e.g. bubble formation in liquids). ψ_p might then be calculated under the assumption that the rest of the system constitutes an external field (including electron exchange terms, etc.) for the particles in Ps. This external field must be derived from the atomic positions and ψ_1. The calculation may, of course, be done in a self-

consistent way. However, such a calculation of the Ps state in condensed matter seems to be a very difficult task at present, and many approximation schemes are possible (see below). Hodges et al.[23] calculated the Ps wave function in quartz and ice by assuming that ψ_p is orthogonal in the electron coordinate to the wave function for the electrons of the solid in the independent particle approximation, and by disregarding Coulomb forces. It is very difficult for us to see why the Ps-electron should be orthogonal to the other electrons, because its motion is dominated by the Coulomb potential of the positron, and not by the lattice potential, which mainly influences the other electrons.

The "spin-averaged" annihilation probabilities (13) and (14) are calculated under the assumption that the spins of the Ps electron and positron are not correlated with the spins of the other electrons. This is not necessarily a good approximation. In particular, the density at the positron of electrons with the spin parallel to the Ps-electron spin is expected to be lower than that of electrons with the opposite spin direction, because the Pauli principle, roughly speaking, introduces a repulsion between electrons with the same spin direction. As 2-γ annihilation only occurs if the positron and electron spins have opposite directions, we therefore expect the para-Ps pick-off rate to be lower than that of ortho-Ps. A calculation of this effect probably has to take into account the correlation effects in a fairly detailed way, i.e. it has to be better than a Hartree-Fock type of calculation. Hence, we certainly cannot estimate this effect here. Intuitively, we expect the greatest difference in pick-off rates in cases, such as quartz and ice, where the pick-off rates are large. Apparently this pick-off effect has not been discussed before. In the literature (e.g. refs. 1-6, 46, 55) the two pick-off rates have not been distinguished. The effect will be further discussed in section 5.

The contributions of the two exchange terms in (12), (13), and (14) relative to those of the well-known intrinsic and pick-off terms are very difficult to estimate. A reasonably correct calculation probably has to include correlation effects. Apparently, Ps is normally repelled by the molecules or atoms of condensed matter (Ps-molecule bound states have been found in special cases). Because Ps sits in a bubble in most liquids, it is probably pressed into the outer parts of the electron

clouds in condensed matter. The positron can penetrate the outer electron shells, and it is repelled only by the positive cores of the atoms. The Ps-electron is normally repelled by the outer electrons too as a result of the Coulomb and exchange forces. Hence, the normally found repulsion between Ps and atoms or molecules is mainly caused by the fact that the positron must be accomponied by the electron when it penetrates the outer electron shells. We therefore expect that the Ps-electron overlap of the other electrons is small compared to that of the positron. It is very difficult to estimate how much smaller it is. Intuitively, we expect that the exchange terms in (12), (13), and (14) are much smaller than the pick-off term, and that they are more important in cases where the pick-off rates are large, i.e. where Ps seems to be strongly "pressed" (as in quartz and ice). They are probably less important in liquids, where the atoms yield to the Ps "pressure" and form bubbles around Ps.

4.3. Models of the Positronium State

In the remainder of this section we shall discuss specific models of the Ps state. In most liquids and solids Ps is localized (except for fairly slow diffusion that may be somewhat enhanced due to tunneling) at the annihilation. In liquids, Ps is normally localized in the bubble, while trapping in defects probably causes the Ps localization in solids, althouth Ps may perhaps also be trapped by digging its own potential well in some solids. A simple model of the localized Ps state is to assume that Ps is bound in an anisotropic (in solids) harmonic potential. First, we assume that

$$\psi_2(\bar{r}_1,\bar{r}_p) = \psi_c(\bar{r})f(\bar{R}), \tag{15}$$

i.e. a product of a function $\psi_c(\bar{r})$ of the center-of-mass coordinate $\bar{r} = (\bar{r}_1 + \bar{r}_p)/2$ and a function $f(\bar{R})$ of the relative coordinate $\bar{R} = \bar{r}_1 - \bar{r}_p$ (e.g. an s-state wave function). Hence, the intrinsic para-Ps term in (13) gives

$$dw \propto \left| \int d\bar{r} e^{-i\bar{k}\cdot\bar{r}} \psi_c(\bar{r}) \right|^2 d\bar{k}d\Omega \tag{16}$$

We further assume that $\psi_c(\bar{r})$ is the harmonic potential wave function of lowest energy E_o. It is easy to show that we obtain a Gaussian linear-slit angular correlation curve for the z-direction of fwhm = Γ_θ, for which $\Gamma_\theta \cdot \Gamma_z = 10.7$ mrad·Å, where Γ_z is the fwhm of the probability distribution of the z-component of $\bar{r}$. We also find $E_o = 16/\Gamma_z^2$ eV (Γ_z in Å). These results are, of course, only applicable if $E_o >> k_B T$. Because $\Gamma_\theta \approx 2.5 - 4$ mrad, which gives $E_o \approx 1 - 2.2$ eV, this is normally fulfilled.

This model illustrates that the shape of the localized para-Ps intrinsic annihilation contribution to the measured angular correlation curve is mainly determined by the zero point Ps center-of-mass motion. Other localized Ps models have been used (see e.g. ref. 56). It is important to realize that the localized Ps wave function may well be significantly different from zero at appreciable distances from the trap, if Ps is weakly bound in the trap. At high enough trap concentration, the wave function may then overlap several traps at the same time, i.e. Ps is delocalized on the traps within its coherence length (see below).

The simple case of a completely delocalized Ps atom was discussed in ref. 19. It was shown that expression (15) and the assumption that $\psi_c(\bar{r})$ is a Bloch function, i.e. that

$$\psi_c(\bar{r}) = e^{i\bar{p}\cdot\bar{r}} \sum_{\bar{g}} a_{\bar{g}} e^{i\bar{g}\cdot\bar{r}} \qquad (17)$$

where $\bar{p}$ is the crystal wave vector and $\bar{g}$ a vector in the reciprocal lattice, gave the intrinsic para-Ps contribution (expression (13))

$$dw \propto \sum_{\bar{g}} |a_{\bar{g}}|^2 \, \delta(\bar{p}-\bar{k}+\bar{g}) \, d\bar{k}d\Omega \qquad (18)$$

As discussed in ref. 19 this explains the presence of the side peaks at angles $\theta = \hbar g_z/mc$ in the angular correlation curves of ice (see figs. 1-3), where g_z is the projection of $\bar{g}$ at the z-direction of the setup (see fig. 4).

It is important to realize that Ps (like electrons in metals) is not delocalized over the whole crystal. Ps will,

of course, be scattered by lattice imperfections (phonons and defects) and hence its wave function will not be coherent over distances that are long compared to the Ps mean free path. A more realistic model would be to consider a Ps state delocalized only within a certain region, the size of which is given by a parameter, the coherence length. In a more complete independent particle theory, the statistical aspects of the problem can of course be introduced by use of the Ps density matrix.

We shall now extend the calculation to take into account the influence of the thermal motion of the atoms on the Ps Bloch function state. The temperature dependence of the electron Bloch function has been treated in the nearly-free-electron approximation by Kasowski[57]. We shall here calculate the para-Ps intrinsic annihilation probability by use of a similar theory of the Ps Bloch function. We assume the Born-Oppenheimer approximation to be valid for the Ps center-of-mass state. Further, we assume that the effective potential seen by the Ps atom is "small", so that we can calculate the wave function for the "frozen-in" configuration of the atoms by use of perturbation theory, the unperturbed wave functions being the free-Ps states. The Ps center-of-mass wave function is therefore a function $\psi_c(\bar{r},\bar{R}_{\ell m})$ of the coordinate $\bar{R}_{\ell m}$ of the m'th atom in the ℓ'th unit cell. We can write $\bar{R}_{\ell m} = \bar{R}^o_{\ell m} + \bar{Y}_{\ell m}$, where $\bar{R}^o_{\ell m}$ is the equilibrium position and $\bar{Y}_{\ell m}$ the displacement from equilibrium.

In the nearly-free-Ps approximation we have

$$\psi_c(\bar{r},\bar{R}_{\ell m}) = |\bar{p}\rangle + \sum_{\bar{p}'}{}' \frac{\langle \bar{p}'|V|\bar{p}\rangle}{(E^o_{\bar{p}} - E^o_{\bar{p}'})} |p'\rangle \qquad (19)$$

$|\bar{p}\rangle$ is the normalized free state, i.e. $|\bar{p}\rangle = (V_o)^{-\frac{1}{2}} e^{i\bar{p}\cdot\bar{r}}$, where V_o is the normalization volume, and $\bar{p}$ the momentum ($\hbar = 1$). $E^o_{\bar{p}}$ is the energy $E^o_{\bar{p}} = |\bar{p}|^2/2M$, where M is the Ps mass. The potential V is assumed to be a sum of atom potentials, whose shapes are independent of the atomic positions

$$V = \sum_{\ell m} v_m(\bar{r} - \bar{R}_{\ell m}) \qquad (20)$$

We shall not discuss the calculation in detail since it is very similar to that found in ref. 57, and e.g. to the calcu-

lation of the influence of phonons on X-ray scattering (e.g. ref. 58). On substituting (19) and (20) into (16) we find an expression for dw in terms of the Fourier components of $\psi_c(\bar{r},\bar{R}_{\ell m})$, which depend on $\bar{Y}_{\ell m}$ the displacement from equilibrium of the ℓm'th atom. $\bar{Y}_{\ell m}$ is calculated in the phonon theory, which therefore can be used to derive the ensemble average of dw with respect to the phonon variables by use of (see ref. 58)

$$<e^{i(\bar{p}-\bar{p}')\cdot(\bar{Y}_{\ell m}-\bar{Y}_{\ell' m'})}>_{av.} \simeq e^{-W_m}e^{-W_{m'}},$$

where e^{-W_m} is the Debye-Waller factor. Finally, we find

$$dw \propto \{\delta_{\bar{p},\bar{k}} + \sum_{\bar{g}\neq\bar{0}} \frac{4N^2M^2}{(|\bar{p}|^2-|\bar{k}|^2)^2 V_o^2} |F|^2 \delta_{(\bar{k}-\bar{p}),\bar{g}}\} d\bar{k}d\Omega \quad (21)$$

where N is the number of unit cells, and the structure factor F is

$$F = \sum_m <\bar{k}|v_m|\bar{p}> e^{-W_m} e^{i(\bar{p}-\bar{k})\cdot\bar{R}_m^o} \quad (22)$$

The wave vector, which must be used in the calculation of W_m (see ref. 58) is $\bar{k}-\bar{p}$. We put $\bar{R}_{\ell m}^o = \bar{R}_\ell^o + \bar{R}_m^o$, where $\bar{R}_m^o$ is the equilibrium coordinate of the m'th atom with respect to the origin of the unit cell. A linear slit setup determines the distribution

$$dw_1 \propto (\int_{2\pi} d\Omega \int dk_x \int dk_y \sum_{\bar{p}} s(\bar{p}) dw(\bar{p},\bar{k}))dk_z \quad (23)$$

where $s(\bar{p})$ is the probability that the state $\bar{p}$ is occupied (e.g. a Boltzman distribution). Normally, Ps is thermalized at the annihilation, i.e. $|\bar{p}| << |\bar{g}|$ for $\bar{g} \neq \bar{0}$. Clearly we again find side peaks at $\theta = \hbar g_z/mc$, as in the simple model discussed above. The intensity of the side peaks is mainly determined by $|F|^2$, which varies with temperature through the Debye-Waller factors.

As expected, the theory of the intrinsic 2-γ annihilation of the para-Ps Bloch function state in the nearly-free-Ps approximation resembles the theories of other well-known diffraction phenomena (e.g. Bragg reflection). To our knowledge, the

best available theories of the temperature dependence of the Bloch function are very similar to the theory we have used here. They are mainly used in the band structure calculations of e.g. Knight shift[57], optical absorption, etc., where the temperature effect is normally approximated by multiplying matrix elements between OPW electron wave functions by the Debye-Waller factors. We shall use the expression derived above on the ice case in section 5.

Clearly, if the center-of-mass Ps wave function is a Bloch function, also the third term in expression (13) contributes to the side peaks. However, in this contribution the side peaks are reduced compared to the narrow central peak because they are weighed with the Fourier transform of the "pick-off overlap" at $\bar{k} = \bar{g}$. Of cource, the influence of phonons on the side peak contributions of the third term can be derived as done above for the first term. The side peak intensities are now determined by the structure factor F (not $|F|^2$) in the first part and by F^* in the second part of the third term.

The trapping of positrons in defects in metals is normally analyzed in terms of the so-called "trapping model"[3,35]. The main assumptions used in this model are 1) the positrons annihilate either from a localized or from a delocalized state, 2) at time zero, the positrons are in the delocalized (bulk) states, and 3) the positrons are trapped with a certain trapping probability per unit time. Stoneham (ref. 59, chapter 14) discusses the trapping processes of electrons in solids and the similar electron trapping model (ref. 59, section 14.5). We shall discuss the application of the trapping model to Ps trapping in ice in section 5.5, where the main conclusion is that a simple trapping model cannot explain our results.

We have therefore also considered a more complicated model of the Ps center-of-mass wave function, namely a "linear combination" model

$$\psi_c(\bar{r}) = c_l\psi_l(\bar{r}) + c_d\psi_d(\bar{r}), \qquad (24)$$

where c_l and c_d are constants. $\psi_l(\bar{r})$ is a localized wave function, i.e. $\psi_l(\bar{r})$ gives, roughly speaking, the wiggles of $\psi_c(\bar{r})$ in or close to the trap. $\psi_d(\bar{r})$ describes a Block function part (different from zero within the coherence length) of $\psi_c(\bar{r})$.

Hence, we consider a case where Ps is delocalized but with a certain degree of localization at the traps (not just either localized or delocalized as described by the "trapping" model). Physically, this model might be a reasonable approximation if a) Ps is not bound in the traps but only influenced by scattering in the traps (resonance scattering, virtual states), - for example if Ps cannot relax fast enough into the ground state of the trap - or b) the Ps wave function penetrates far outside the trap and, for example, is trapped in several traps at the same time at a high enough trap concentration.

On substituting (24) into the first term in (13) we get

$$dw \propto \Big[|c_\ell|^2 \left| \int e^{-i\bar{k}\cdot\bar{r}} \psi_\ell(\bar{r}) d\bar{r} \right|^2 + |c_d|^2 \left| \int e^{-i\bar{k}\cdot\bar{r}} \psi_d(\bar{r}) d\bar{r} \right|^2$$

$$+ \left\{ c_\ell^* c_d \left(\int e^{-i\bar{k}\cdot\bar{r}} \psi_\ell(\bar{r}) d\bar{r} \right)^* \int e^{-i\bar{k}\cdot\bar{r}} \psi_d(\bar{r}) d\bar{r} \right\} + \left\{ --- \right\}^* \Big] d\bar{k} d\Omega \tag{25}$$

Clearly, if $\psi_d(\bar{r})$ is a Bloch function we get narrow peaks also from the last two "interference" terms in (25). However, the side peak contributions of these terms are very small as they are weighed by the Fourier transform of $\psi_\ell(\bar{r})$, which normally is very small at $\bar{k} = \bar{g} (\bar{g} \neq \bar{0})$. Hence the "interference" terms contributes significantly only to the narrow central peak. We also calculated the influence of phonons on the "interference" terms. However, the narrow central peak is not influenced by the phonons in the nearly-free-Ps approximation, and hence the phonon influence is negligible in this case. Actually, the "interference" terms are probably small compared to the first two terms, because their total contribution is given by the overlap of ψ_ℓ and ψ_d, which is probably small in most cases (the normally found concentration of traps is of the order of 10 ppm).

Disregarding the interference terms, we find for the total intrinsic annihilation decay rate

$$w = \tau^{-1} = |c_\ell|^2 w_\ell + |c_d|^2 w_d, \tag{26}$$

where w_ℓ (w_d) is the decay rate of the localized (delocalized)

state alone, and τ is the lifetime. On substituting (24) into the pick-off term in (14),we again get two "interference" terms, whose total contributions are determined by the common overlap of the delocalized Ps positron, the localized Ps positron, and the system electrons. Hence, the "interference" pick-off terms may be neglected compared with the other pick-off terms, and the pick-off decay rate is then given by an equation similar to (26), where $w_\ell (w_d)$ now are the pick-off rates of the localized (delocalized) states alone. A similar expression is found for free positron annihilation by use of a linear combination of a localized and delocalized positron wave function multiplied by a many-electron wave function in expression (10), and on neglecting "interference" terms. The "linear combination" model (24), which gives the decay rate (26) in these three important cases, is of importance as an alternative model to the trapping model[3,35] normally used to explain positron trapping in metals (see ref. 60 for a mainly classical discussion of the "linear combination" model).

Difficult problems in the application of the "linear combination" model will be to find a reasonable assumption for the values of the coefficients c_ℓ and c_d and for w_ℓ and w_d as function of the trap concentration. In a first approximation w_ℓ and w_d can probably be considered to be constants equal to the decay rates measured at high and low defect concentration, respectively. A quantum mechanical calculation of the wave function for randomly distributed, simple potential wells might be used to solve this problem in an approximate way. We shall further discuss this model in the next section.

5. DISCUSSION

5.1. General Remarks

In this section a fairly detailed discussion of positronium in ice will be given. Since the various topics treated in this discussion are closely interrelated, there is no obvious way of arranging them. For example, Ps-trapping in vacancies is a good argument for the high vacancy concentration in ice at the melting point. On the other hand, Ps-trapping is also experimental evidence of the formation of Ps in ice. Hence, the

discussion is somewhat arbitrarily organized in the following way. At first we discuss the evidence of the presence of Ps in ice. Secondly, a short discussion of Ps formation is given, followed by a detailed treatment of the Ps Bloch function. We then discuss in detail the evidence for Ps-trapping in vacancies, and the use of different models of the influence of vacancies on the Ps state for the interpretation of our results. The high vacancy concentration implied by our results and the interpretation as well as its importance for other branches of ice physics, is next discussed, followed by some remarks on miscellaneous topics at the end of this section.

5.2. Evidence for Positronium in Ice

Before we enter into a more detailed discussion of our data, it is worth considering critically the most important aspect of the interpretation of the results, that is the nature of the positron state in ice - which we call a Ps state. In other words, what is the evidence for the presence of positronium in ice? Of course, this question cannot be answered before solving a semantic problem, namely the definition of a Ps state. Obviously, the pure Ps state is only found in vacuum. Any overlap of the wave functions of the Ps electron and/or positron with the wave function of other electrons, or any forces due to the presence of other electrons (e.g. polarisation (van der Waal) forces) and/or ions will, in principle, change the Ps wave function away from a pure Ps state. On the other hand, experimental results show that the positron is found in a state with properties similar to the pure Ps state in many liquids and solids. The most important deviation from the pure Ps state is the finite pick-off annihilation rate. If the pick-off lifetime, τ_p, is shorter than about 1 nsec, in particular if it is comparable to the free positron lifetime of 0.4 - 0.5 nsec, we expect the Ps state to deviate appreciably from the pure Ps state. This occurs in ionic crystals, quartz ($\tau_p \lesssim 0.4$ nsec), and in ice ($\tau_p = 0.67$ nsec). A narrow component (fwhm $\lesssim 4$ mrad) in the angular correlation curve, resulting from para-Ps intrinsic annihilation in the bubble state in liquids or in a delocalized or localized (trapped in a defect) state in a solid, is also strong indication of the presence of a positron state fairly similar to the pure Ps state. If Ps is present, a mag-

netic field will reduce the long lifetime and increase the intensity of the narrow components[1,4,22,33,61]. This magnetic field effect is very specific for Ps. If these (and other) experimental attributes of Ps are found, we say that Ps (i.e. a somewhat distorted pure Ps state) is present in our system. The wave function for the total system of Ps plus electrons is probably fairly well represented by the wave function (11), or even by the simpler, more approximate wave function where the antisymmetry operator is removed from (11). The experimental results show very clearly that Ps, in the above definition, is present in ice. The long lifetimes, 0.67 - 1.2 nsec, found in pure and doped ice are too long to be explainable in terms of free positron annihilation. They can only arise as a result of the ortho-Ps pick-off process. The narrow central peak and side peaks must be due to annihilation of an electron-positron pair with a center-of-mass momentum corresponding to thermalized or almost thermalized Ps. Recent angular correlation results for ice show that thermalization takes place even at liquid helium temperatures[62]. Considering that a short lifetime of roughly 125 psec, which cannot be explained in terms of free positron annihilation, has been found in ice[18], the only reasonable explanation is that the peaks are due to para-Ps decay. Furthermore, the magnetic field effect has been found in polycrystalline ice[4,33,61]. As mentioned in section 3 the fact that the very detailed analysis of our results in terms of Ps states is self-consistent, also constitutes a fairly detailed test of the presence of Ps in ice. Finally, it may be mentioned that the narrow central peaks and side peaks found in quartz have been successfully interpreted in terms of delocalized Ps[22,23]. In particular, a detailed magnetic field effect measurement on quartz single crystals strongly indicates the presence of Ps[22]. We can conclude that the available experimental results show very clearly that Ps is present in ice. As it is somewhat difficult to interpret Ps trapping in ice, as we shall see later, this conclusion is important.

5.3. Positronium Yield in Ice

The intensity of the narrow peaks, I_N, was found to be 16.34 ± 0.2 %. The uncertainty of ±0.2% is a rough estimate

based on five independent measurements (two a-axis and three c-axis curves). This value may contain some errors if the corrections for annihilation in the sample box walls (subtraction of a mainly broad curve of 7.3% intensity, see section 3) are somewhat inaccurate. For example, if only 6.3% was subtracted, the narrow peak intensity would decrease by 0.16% to 16.18%. This intensity corresponds to a para-Ps intrinsic annihilation. If we assume that the para-Ps and ortho-Ps have the same pick-off annihilation rates, we get the total para-Ps yield

$$I_p = 16.34 \cdot (\lambda_0 + \lambda_{pb})/\lambda_0 = 19.4\%$$

(compare expression (1)), which gives an ortho-Ps yield of $I_o = 3I_p = 58.2\%$. However, the ortho-Ps yield determined as the long-lifetime intensity I_3 for HF doped ice is only $54 \pm 2\%$[18,31]. The difference between this value and $I_o = 3I_p$ is probably significant, even if we take into account uncertainties on the determinations of I_p and I_3. Several possible explanations of this fact may be proposed. A para-Ps pick-off rate of only half that of ortho-Ps can explain the difference. As discussed in section 4, we theoretically expect the para-Ps pick-off rate to be lower than that of ortho-Ps. Another possible explanation is that the ratio of the ortho-Ps to the para-Ps yields is not 3 to 1, but somewhat lower. We have found that the long lifetime intensity is significantly smaller than three times the narrow component intensity in several non-polar liquids, if the narrow component is defined as the narrowest (fwhm ≈ 2.5 mrad) Gaussian in a three Gaussian fit of the angular correlation curves. It is important to realize that the ortho- to para-Ps ratio has only been determined with rather large uncertainty hitherto, mainly because of the difficulties in extracting the para-Ps yield from the measured results. Our determination of the para-Ps yield is unusually precise because of the very narrow central and side peaks found.

In subsection 4.1 we discussed the spur process of Ps formation. Since very little is known from radiation chemistry research about electron spurs and electron behaviour in ice, compared to the knowledge available of typical liquids, we can only give some speculative comments on Ps formation here. In liquids, a fairly clear correlation has been found between the

electron mobility μ and the Ps yield[44,63,64]. High μ-values correspond to high Ps yields. Except for liquid tetramethylsilane[64] (TMS, I_3 = 55%), the long-lifetime intensity for ice is the largest found in condensed matter. Recently, the electron mobility μ in ice has been found[65] to be μ = 1 - 10 cm^2 V^{-1} sec^{-1}, a fairly large value, which roughly agrees with the correlation between μ and the Ps yield found in liquids. One might imagine that the spur size in ice is comparable to that in TMS and neopentane (radius ≈ 200 Å), which, together with the high electron mobility, explains the effective Ps inhibition by radicals created by γ-radiation in ice[32]. Actually, we found a small decrease in the intensity of the narrow components ($\Delta I_N \approx -0.6\%$) in some very pure single crystal samples (from J. Bilgram) exposed to positron radiation from the source for 9 days at ≈ -180°C. A calculation, in which Ps-inhibition and a yield of inhibiting species of 0.2 species/100 eV deposited energy (the H_2O_2 yield measured in ref. 66) were assumed and the inhomogeneous distribution of radiation damage taken into account, gave an inhibition constant of $\sigma \approx 370$ M^{-1} for $I_N(c) = I_N(0)/(1 + \sigma c)$, where c is the specie concentration. A probably better determined value of σ = 450 M^{-1} has been derived from the γ-irradiated ice results discussed in ref. 32. These σ-values are roughly 2-3 times larger than the largest values found in liquids[48,67]. However, a large σ-value is expected if the spur size and electron mobility are large. As shown in ref. 32, the Ps inhibiting species anneal out at temperatures above roughly -180°C. This annealing and the shorter irradiation times are probably the reasons why we saw no significant Ps inhibition in other measurements. The accumulation of radiation damage might be one of the reasons why very few cases of delocalized Ps have been found.

The spur model of Ps formation[44,45,64] predicts that Ps is normally formed by thermalized electrons and positrons, i.e. Ps is formed in a thermalized state with respect to the center-of-mass degrees of freedom if its zero point energy is small compared to kT. The fact that the narrow central peak at liquid helium temperature[62] and at the temperatures of our experiments[19] can only be explained by a thermalized or nearly thermalized electron-positron pair is therefore in good agreement with the spur model of Ps formation. In the analysis of

the curves discussed in section 3, we assumed that the total probability of para-Ps formation is independent of temperature. We calculated the intensity of the broad component, I_B, corrected for the change in the para-Ps pick-off rate due to Ps-trapping. This correction was $\Delta I_B = 0.7\%$ from -180^oC to -1^oC (see table 2). As illustrated in Figs. 2 and 3, the subtraction of this broad component reduces the counts to zero at angles where the para-Ps components vanish for all temperatures. This clearly shows that our assumption of the temperature independence of the para-Ps yield agrees very well with the experimental facts.

A possible model of Ps localization is to assume that Ps is formed in the vacancies, i.e. that one of the particles is initially trapped in a vacancy followed by a trapping of the other particle to form trapped Ps. However, this model is unlikely because it predicts that the Ps yield is temperature dependent, in marked disagreement with experimental facts.

We have until now discussed the Ps inhibition in the positron spur by radicals created by the preceding positron radiation. Similarly, Ps may be trapped by vacancies created by the preceding positron radiation[32,62]. As discussed above, these effects are very small at temperatures above -180^oC. However, spur defects (ions, radicals, vacancies, etc.) created by the positron that forms Ps influence the Ps yield. Hence, it is appropriate here shortly to discuss the possibility that the temperature dependence of the Ps trapping is a result of temperature dependent spur processes. In section 5.5 we then return to a more detailed discussion of the trapping of Ps in homogeneously distributed vacancies.

As the measured Ps yield is temperature independent, we can conclude that the processes (e.g. electron-ion recombination, out-diffusion, etc.) that mainly influence the Ps yield are either roughly temperature independent or vary with temperature in such a way that the Ps yield is kept constant. The next question is whether Ps becomes trapped in spur vacancies, i.e. the vacancies created by the positron that forms Ps in the spur. At low temperature the yield of vacancies is roughly one vacancy per 100 eV loss of positron or electron energy[32,66]. Such a high yield cannot be explained in terms of the direct positron or electron collisions with the atoms (recoil effect) but must

be caused by the effects of the electronic damage (ionizations, excitations, etc.), as is normally the case in systems studied in radiation chemistry (compare also F-center formation in e.g. KCl). Probably the vacancies are mainly formed as one (out of several possible) result of the electron-ion recombination and/or the electron-radical reactions. The vacancy is probably formed in times comparable to or longer than the Ps formation time. Two models of Ps trapping in spur vacancies might be considered, namely that 1) Ps is trapped in a spur vacancy created by other processes (recombination, etc.) than the Ps formation itself, and 2) Ps is trapped in a vacancy created by the Ps formation process (i.e. that part of the Ps binding energy may be used to form the spur vacancy, that trap Ps). Both models (and other, more complex models) are unlikely because they predict that the Ps yield would be strongly temperature dependent in clear disagreement with experimental facts, if it is assumed that the Ps trapping in spur vacancies causes the measured, strong temperature effects. Regarding model 1, it is very difficult to explain the fairly high degree of Ps trapping ($\simeq$ 65% at -1^{o}C) on taking into account that a) spur vacancies are not expected to be formed in all positron spurs, b) many spur vacancies are probably created after the Ps is formed, c) the spurs are expected to be fairly large, and d) an appreciable amount of the positrons ($\simeq$ 25%) and the electrons (free electron yield ($\simeq$ 1 per 100 eV) escape from the spurs, which suggests that a much greater amount of the neutral Ps atoms might escape the trapping in the neutral vacancies. Concerning the model 2, it is difficult to explain a strong temperature effect in terms of this model as the Ps binding energy in ice is much bigger than the thermal energy kT.

In summary, the Ps trapping in spur vacancies can very probably not explain the measured Ps trapping effects. On the other hand, the Ps trapping is fairly well explained as trapping in temperature created vacancies, as will be discussed in detail below. It must be emphasized that the given discussion of the spur processes is necessarily provisional because little is known about the details of the radiation damage in ice.

5.4. The Positronium Bloch Function

In section 4 the theory of the annihilation from a Ps Bloch function state was discussed. To obtain the side peaks it is not necessary that the Ps wave function is separable into a center-of-mass and a relative coordinate wave function, as given in (15). The only necessary condition is that $\psi_2(\bar{r}_1, \bar{r}_1)$ in (13) is a Bloch function. However, $\psi_2(\bar{r}_1, \bar{r}_1)$ is probably separable in a fairly good approximation, because its properties are close to those of the pure Ps state (e.g. the strength of the magnetic field effect[33,61]). In the following we will therefore argue in terms of the center-of-mass wave function $\psi_c(\bar{r})$. In ice, hydrogen atoms are disordered on hydrogen bonds[10,42]. Hence, even if we disregard the thermal motion of the atoms (including the zero point energy effect), the symmetry of the Ps potential in an independent Ps model is not the translation symmetry of the ice lattice, and in principle the Ps wave function $\psi_c(\bar{r})$ is not a Bloch function. However, $\psi_c(\bar{r})$ may not be very different from a Bloch function, as the potential from hydrogen is probably much smaller than the oxygen part of the potential. It might also be argued that the Ps potential is probably little changed when a proton is moved from one position to the other on a hydrogen bond. Hence, at first we assume in the following discussion that we have a Ps Bloch function, and we later return to the proton disorder problem. The possibility that $\psi_c(\bar{r})$ is a linear combination of a Bloch function and a trapped Ps function will also be discussed later. In table 3 are shown the contributions to the angular correlation curve at the reciprocal lattice points, $\bar{g}$. According to our interpretation, they are given by $\sum_{\bar{p}} s(\bar{p}) |a_{\bar{g}}(\bar{p})|^2$, where $s(\bar{p})$ has been defined in (23), and $a_{\bar{g}}(\bar{p})$ (see (17)) is the Fourier transform of $\psi_c(\bar{r})$ at $\bar{g} + \bar{p}$. We may assume in a fairly good approximation that $a_{\bar{g}}(\bar{p})$ is roughly independent of $\bar{p}$ in the region where $s(\bar{p})$ differs from zero. Hence, contributions A to D in table 3 are simply proportional to $|a_{\bar{g}}|^2$, i.e. we can measure the numerical value of the Fourier transform of $\psi_c(\bar{r})$. The phases of $a_{\bar{g}}$ are not determined. Of course, this is the maximum information available in a momentum measurement. As expected, the Fourier transform only differs from zero for the $\bar{g}$ vectors close to zero. The structure factor given in table 3

Table 3

The contribution to the angular correlation curves at the reciprocal lattice points correlated with the structure factor and the distance to the origin. In cases where several points have equal contributions and structure factors, only one set of coordinates is shown (e.g. the (1,0,0) type points).

Coordinates	Name	Contribution (%)	Structure factor $\|F_o\|^2$	Distance (mrad)
(0,0,0)	C	11.393	-	0
(0,0,±1)	-	≈ 0	0	3.315
(1,0,0)	A	0.536	4	6.233
(0,0,±2)	D	0.585	8	6.630
(1,0,±1)	B	0.0466	1.75	7.060
(1,0,±2)	-	≈ 0	2	8.884
(1,1,0)	-	≈ 0	16	10.796

is $|F_o|^2 = |\sum_m \exp(-i\bar{g}.\bar{R}_m^o)|^2$, where the summation is over the four oxygen positions in the unit cell. In terms of the nearly free Ps theory discussed in section 4, this corresponds to the assumption that the total Ps potential results from the presence of the oxygen atoms (ions), and that $\langle\bar{k}|v_m|\bar{p}\rangle \exp(-W_m)$ in (22) is the same for all four oxygen positions. As seen in table 3, the effect of the structure factor explains why $a_{\bar{g}}$ is zero for $\bar{g} = (0,0,\pm 1)$. It may also explain why D is enhanced compared to what is expected if only the effect of the distance to the origin is considered.

The influence of the thermal motion of the atoms on the Ps wave function was discussed in section 4 in terms of the nearly free Ps model. As shown in (21) and (22), $|a_{\bar{g}}|^2 \propto \exp(-2W)$, if W_m is roughly independent of m (as is the case for the ice oxygen atoms[68]). The measured Debye-Waller factors, W_m, are fairly well described by the Debye approximation with a Debye temperature[10,42] $\theta = 224^oK$, which gives $\exp(-2W) = 0.956$ (0.889) at -180^oC (-1^oC) for the (1,0,0) points (A) and $\exp(-2W) = 0.950$ (0.876) for the (0,0,±2) points (D). This gives a reduction of

A of 7% (and of D of 8%) in the temperature interval -180°C to -1°C. We may reasonably assume that the reduction in the (0,0,0) contribution (C) for increasing temperature (see Figs. 6 and 7) results from the trapping of Ps in vacancies. The extra reduction, measured for A and D, is then reasonably ascribed to the influence of thermal motion on the Ps wave function. This interpretation is in agreement with the fact that A, D, and C are reduced the same amount when HF is added to ice at low temperatures[31]. Probably HF-doping strongly increases the vacancy concentration at lower temperatures. The measured A, D, and C values at -1°C are 0.26, 0.15, and 0.40 times the values at -180°C. Hence, the measured reduction in A (D) relative to the C-value is 35% (62%). In other words, our measurements indicate that roughly 65% of the para-Ps atoms are trapped at -1°C, and that the Fourier transforms at $\bar{g} \neq \bar{0}$ are reduced appreciably relative to that at $\bar{g} = \bar{0}$ for the about 35% of the para-Ps atoms annihilating from an approximate Bloch function state compared to the situation at -180°C. Clearly, the measured reductions in A and D relative to C cannot be explained in terms of the theory developed in section 4. Not only the magnitudes, but also the functional form of the measured reductions versus temperature, differ from the predictions of the theory. Of course, the A, D, and C values may contain some small errors due to the uncertainties of the analysis, as described in section 3. However, such errors are much too small to explain the failure of the Debye-Waller factor theory. The discrepancy between the simple nearly-free-Ps theory and the experimental results may be explained in different ways. 1) The nearly-free-Ps theory may be too simple. 2) The disorder on the hydrogen bonds may cause a much stronger temperature dependence of the Ps wave function than that found in perfect crystals. 3) The ion-state and orientational (Bjerrum) defects, the concentrations of which increase roughly exponentially with temperature[10,42], might influence the delocalized Ps state, even if none of them seems to trap Ps. 4) Similarly, the presence of vacancies might also influence the delocalized Ps state (apart from the effect of trapping). 5) Ps might be in a state that is roughly a linear combination of a delocalized and a trapped state (see subsection 4.3), and maybe the delocalized state component is strongly influenced by the thermal motion of

the atoms through the influence on penetration distance of the Ps wave function outside a trap (a coherence length effect).

We have discussed the Ps wave function in some detail partly because similar detailed information about the wave function in an independent particle model seems unavailable for the two other light particles that participate in normal low energy physics, namely the electron and the positron. For example, in the presently available experimental results it is extremely difficult to distinguish between the true and the pseudo wave function in the case of electrons in metals and semiconductors, although these wave functions are very different indeed. Only quantities, such as the shape of the Fermi surface, optical absorption, and Knight shift, which are not very sensitive to the wave function itself, can be measured. Neither can the positron wave function in an independent particle model be experimentally studied directly. The most detailed measurable quantity is the Fourier transform of the positron-electron overlap, as expressed in (10). Hence, the Ps wave function in solids (and liquids) may be the best system on which various independent particle models can be tested against experiments, a particular case being the temperature dependence of a wave function, that is approximately a Bloch function.

5.5. Positronium Trapping in Vacancies

5.5.1. Introductory Remarks

We have mentioned above that the differences in angular correlation curves and lifetimes between high and low temperatures are mainly caused by trapping of Ps in temperature-created vacancy-type defects. Both the lifetime and angular correlation results give evidence of the trapping, as we shall now discuss in detail.

The increase of the ortho-Ps lifetime τ_3 and the appearance of the τ_4 ($\sim$ 1.7 nsec) component at higher temperatures show that the ortho-Ps atoms tend to become trapped in regions of less than average electron density, i.e. in vacancy-type crystal defects, as was also argued in refs. 18 and 32. In the angular correlation curves the appearance of the middle-broad (3.4 - 3.94 mrad) para-Ps component shows that, at higher temperatures, para-Ps tends to become localized in regions with a size of about 3 Å (subsection 4.3).

In ref. 32 we argued that in γ-irradiated ice Ps becomes trapped in water molecule vacancies in which ortho-Ps has a lifetime of 1.2 nsec. A vancancy formation energy of 0.28±0.07 eV was derived. This activation energy entails a vacancy concentration near the melting point of at least some parts per million (ppm). Simple arguments based on the value of the self-diffusion also lead quite independently to the conclusion that vacancies are present in at least ppm concentration near the melting point[69]. Hence, the vacancy concentration at higher temperatures is so high that vacancies must be expected to act as trapping sites, contrary to previous estimates[18]. Furthermore, the localization of para-Ps within approximately 3 Å mentioned above is in agreement with the dimensions to be expected for trapping in vacancies. So there is strong evidence for associating the τ_3, I_3-lifetime component and the middle-broad angular correlation component with Ps trapping at vacancies. The lifetime of ortho-Ps completely trapped in these thermally created vacnacies is probably close to 1.2 nsec[18,32]. In agreement with the suggested origin of similar long-lived components in refs. 31 and 32, we tentatively propose that the long-lived ($\tau_4 \sim 1.7$ nsec) component is a result of ortho-Ps trapping in divacancies.

5.5.2. The Trapping Model

Positron trapping in vacancies in metals has been studied for some years, and vacancy formation energies have been extracted from these measurements. To do so the "trapping model" has been applied as mentioned earlier. The model relates vacancy concentrations to the observed changes in lifetimes or angular correlation curves, and it has so far been used with reasonable success for positron trapping in metals (see e.g. refs. 3, 7, and 35). Some main features of the model are the following. At zero time, all positrons are in the bulk. From the bulk state they are trapped into vacancies at a constant trapping rate (trapping probability per unit time), which is usually taken proportional to the vacancy concentration. This gives rise to two components in a lifetime spectrum, a longlived one with a lifetime characteristic of a positron in a vacancy and a shortlived one for positrons disappearing (by annihilation or trapping) from the bulk. The intensity of the longlived

component increases with increasing vacancy concentration. Similarly, two components will appear in an angular correlation curve, one from positrons annihilating in the bulk, one from those annihilating in a vacancy.

This simple trapping model cannot account for the observed trapping of Ps into vacancies in ice. In Fig. 5 it is seen that the fraction of para-Ps contributing to the middle-broad component is about 65% close to the melting point. In terms of the trapping model this is the fraction of para-Ps trapped in vacancies. Since ortho-Ps in the bulk ice lives 5-6 times longer than para-Ps, the model predicts that almost all ortho-Ps must be trapped at the melting point (more than 92% of all ortho-Ps will be in the longlived component). Hence, at temperatures close to the melting point, a saturation-like behaviour of an average ortho-Ps lifetime should take place (as seen for positron trapping in many metals[3]). However, this is not observed (subsection 3.2 and ref. 18). Furthermore, the ortho-Ps decay seems to result in only one main lifetime component τ_3 of constant intensity (apart from the low intensity component τ_4, I_4) (subsection 3.2) and not in two components as the simple trapping model requires. Close to the melting point τ_3 is about 1.0 nsec. With the lifetime in a vacancy of 1.2 nsec this suggests that the effective fraction of ortho-Ps trapped is roughly the same as the fraction of trapped para-Ps.

It is possible to account for this by an extension of the simple trapping model to include one more parameter that allows for detrapping of Ps trapped in a vacancy. We therefore set up the trapping model for the following situation[3]. Ps is trapped into vacancies and divacancies with the time independent trapping rates κ and β, respectively. Ps trapped in a vacancy will be detrapped into the bulk with a time-independent escape rate δ. Ps in divacancies will not escape. This extension of the model provides enough parameters for it to be able to reproduce the experimental results. We have used 0.66, 1.2, and 1.7 nsec as the lifetime of ortho-Ps in the bulk, in a vacancy, and in a divacancy, respectively, and assumed the total para- and ortho-Ps yields to be 19.4% and 54%. From the measured values of τ_3, I_4 and the middle-broad component intensity (assumed to include contributions from para-Ps trapped in both mono- and divacancies) κ, β, and δ can be calculated. This was done for the tempera-

tures at which angular correlation measurements were made. (The τ_3 and I_4 values were taken from smoothed curves through the experimental points). The results are shown in Fig. 8 plotted as a function of the inverse temperature. It appears that δ is essentially temperature independent (6 $nsec^{-1}$), while κ is reasonably well approximated with a straight line whose slope is equivalent to an activation energy of 0.2 eV. At the highest temperatures, also β is well approximated by a straight line with a slope of 0.36 eV. Although in principle this two-trap model gives a three component decay for ortho-Ps, the rather high escape rate from the vacancies (and the small β's) entails that at all temperatures almost all ortho-Ps intensity is found in the vacancy component and very little in the shortlived bulk component. Hence, the model gives for ortho-Ps (apart from the τ_4, I_4 component) essentially one component with constant intensity and a lifetime increasing with temperature as found experimentally.

In Fig. 8 the ortho-Ps lifetimes in mono- and divacancies were assumed to be 1.2 and 1.7 nsec. If τ_4 is taken to be 2.3 nsec instead of 1.7 nsec in the analysis (section 3.1 and Ref. 32) the shapes of the curves in Fig. 8 will be unchanged, but the κ values will be slightly smaller, the β values about half, and δ constant at approx. 4 $nsec^{-1}$. The parameters are more sensitive to changes in the assumed ortho-Ps vacancy lifetime, τ_v. For τ_v = 1.1 nsec, δ will decrease to about 0.7 $nsec^{-1}$ at the highest temperatures, while the slopes of κ and β will be approximately 0.19 eV and 0.5 eV. For τ_v = 1.3 nsec, δ will increase to about 10 nsec at the highest temperatures and the slopes of κ and β be approximately 0.23 eV and 0.22 eV.

A tempting interpretation of Fig. 8 would be to assume that κ and β are proportional to the vacancy and divacancy concentrations, respectively. (Explaining the deviation of β from a straight line below $-25^{\circ}C$ as a systematic error in the very small (0.25-0.5%) I_4 values found at these temperatures). This would lead to a vacancy (divacancy) formation energy of 0.2 ± 0.03 eV (0.36 ± 0.14 eV), in reasonable agreement with our earlier estimate[32] of 0.28 ± 0.07 eV for vacancies. For weak binding of divacancies, their formation energy should be about twice the vacancy formation energy, as Fig. 8 suggests. However, the trapping rate per vacancy (or divacancy) need not be temperature

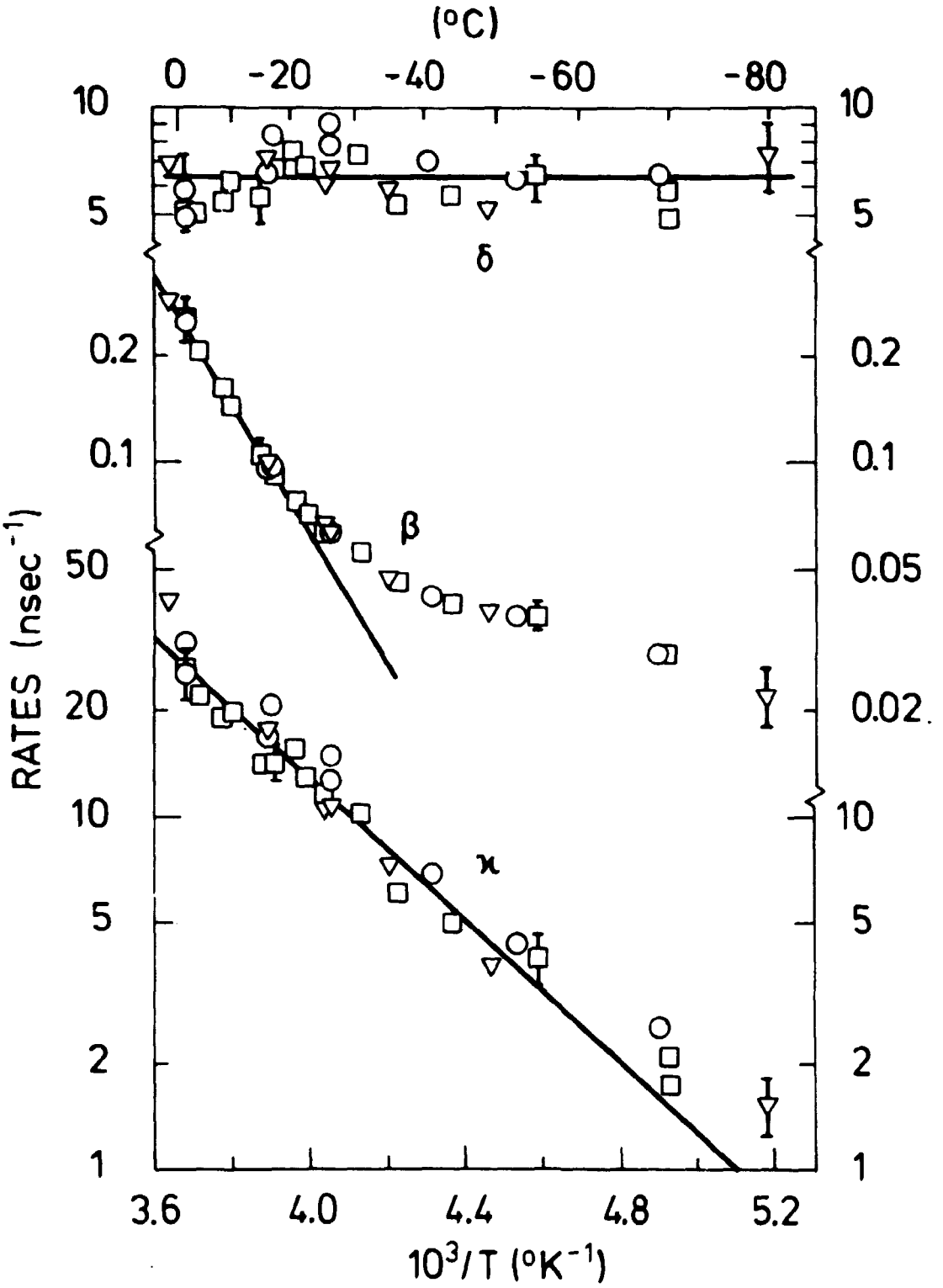

Fig. 8. Parameters extracted from the extended trapping model. κ and β represent the trapping rates into mono- and divacancies, respectively, δ the escape rate from the monovacancies. Squares and circles are for H_2O a- and c-axis crystals, respectively, and the triangles for D_2O c-axis crystals. The pick-off lifetimes used in the calculations were 0.66, 1.2, and 1.7 nsec for the bulk, mono- and divacancies, respectively. The straight lines drawn have slopes equivalent to activation energies of 0.2 eV and 0.36 eV for κ and β, respectively.

independent. Measurements on HF doped ice suggest that the trapping rate per vacancy decreases with increasing temperature[30], as also observed for positron trapping in vacancies in silicon[70]. If so, a larger vacancy formation energy would result.

Usually, when detrapping is considered, it is explained as thermal excitation of the trapped positron (or Ps) out of the trap[71]. The temperature independent δ in Fig. 8 is therefore difficult to understand within the model. To conclude the discussion of the two-trap model with escape, we may say that although it can account for the measured results, this does not necessarily mean that the model gives a correct description of the trapping process for Ps in ice. The main reason is that the inclusion of detrapping in the model provides an (almost) sufficient number of parameters to fit any set of combined lifetime and angular correlation results, but also the constant δ poses a problem.

Seeger[71] pointed out that if the diffusion of Ps to some extent limits the trapping rate into vacancies, the trapping rate will be time-dependent and higher at shorter times. For a completely diffusion-limited trapping, the trapping rate per vacancy is proportional to $1 + r/(\pi Dt)^{\frac{1}{2}}$, where r is the effective radius of the trap, D the Ps diffusion constant and t the time[71]. If the last term is to be of importance, then it must be of the order of unity for times comparable to or longer than that of the para-Ps lifetime ($\sim$ 0.1 nsec). For a given trapping rate, r is in a first approximation inversely proportional to D, as given by the Smoluchowski equation[71]. Hence, for the last term to be unity, t is proportional to r^3. Using numbers for Ps trapping by HF-created defects in ice[18], we find r = 63 Å for t = 0.1 nsec. This radius is probably too large to be realistic[59]. Furthermore, the simple trapping model with a time-dependent trapping rate gives a longlived ortho-Ps vacancy component with a constant lifetime and an intensity that increases with temperature - in apparent disagreement with the lifetime results. Also it is doubtful whether a classical diffusion picture is a good approximation to the behaviour of the delocalized Ps. Thus, the inclusion of a time-dependent trapping rate in the trapping model does not seem to be able to account for the experimental results.

5.5.3. Linear Combination Model

At the end of section 4 we discussed another model, called the linear combination model, in which the Ps center-of-mass has a wave function that is the sum of a delocalized function and a function localized at the monovacancies. This model has the virtue that localization at monovacancies gives rise to a single ortho-Ps lifetime, which increases with vacancy concentration (eq. (26) section 4). Furthermore, since the wave function (eq. (24)) is assumed to be established after a time that is small compared to the para-Ps lifetime, the degree of localization will be the same for ortho- and para-Ps in qualitative agreement with experiments (see above). However, the model does not give a detailed quantitative agreement between the lifetime and angular correlation results as discussed in the following. To account for the longlived ($\sim$ 1.7 nsec) lifetime component, we included in the model also trapping into divacancies from the state given by eq. (24), as described by the simple trapping model[3]. This has only slight influences on the other quantities in the model calculation and is not important for the conclusion. Using eq. (26) for the pick-off annihilation of ortho-Ps, we calculated $|c_\ell|^2$, taking from the lifetime measurements $w = 1/\tau_3$, $w_d^{-1} = 0.66$ nsec, and $w_\ell^{-1} = 1.2$ nsec at all temperatures. We assume that the first term in eq. (25) only gives rise to the middle-broad para-Ps component in the angular correlation curves, while the second term only gives rise to the narrow peaks (ignoring the interference terms). Because for para-Ps $w \approx w_\ell \approx w_d \approx 8 \times 10^9$ sec^{-1}, we find in eq. (26) that the total intensity of the middle-broad component is given by: $I_M = I_p|c_\ell|^2\, w/(\lambda_{po} + w)$, where I_p is the total para-Ps yield, w the intrinsic annihilation rate, and λ_{po} a pick-off annihilation rate for para-Ps. For the values of $|c_\ell|^2$ obtained from the lifetime results, we determined I_M. However, it turned out that this calculated middle-broad component intensity was 2.5-3.5% (i.e. the %-units in Fig. 5) above the measured intensity for all temperatures (Fig. 5). This was true whether λ_{po} was taken as zero or the ortho-Ps pick-off rate, whether I_p was equal to 18 or 19.4% (see section 3), or whether using results from lifetime analyses with $\tau_4 = 1.7$ or 2.3 nsec. Agreement between measured and calculated I_M may be obtained above -20°C if the lifetime of localized ortho-Ps is assumed to be about 2

nsec. This seems an unrealistic value and at lower temperatures it has to be even higher to obtain agreement. Hence, we must conclude that the linear combination model as discussed above and in section 4 does not account for the experimental results. On the other hand, the assumptions about w_ℓ and w_d may be too simple as shortly mentioned in subsection 4.3. If we allow for this by including further parameters in the model, it can, of course, be made to fit the experimental results.

5.5.4. Concluding Remarks

The above discussion of two different simple models for the localization of Ps at vacancies shows that neither the often-used trapping model, nor a linear combination model, can account for the observations unless they are modified by the inclusion of further parameters. These problems arise to some extent from the fact that more experimental information about the localization (trapping) of Ps at vacancies has been obtained than is usually obtained for trapping of positrons in metal defects. In the latter case some information can in principle be obtained about the possible time-dependence of the trapping rate by comparing lifetime and angular correlation measurements, although there seems to be only one example of this having been done[35]. In the case of trapping of Ps, information can be obtained at two different times widely separated, viz. after the para-Ps lifetime ($\sim$ 0.1 nsec) by angular correlation measurements and after the ortho-Ps lifetime ($\sim$ 0.7 nsec) by lifetime measurements. Hence, it is possible to get some information about the development over a rather long period of time of the Ps state from a non-trapped (delocalized) to a trapped (mainly localized) state. A detailed theoretical treatment of the Ps trapping process would be highly desirable, as the present results provide a good experimental material with which to compare such a theory. The above discussion only suggests that trapping does not take place at a constant trapping rate (as assumed in the trapping model), nor does the final - partly localized - state seem to be established in a time that is short compared to the para-Ps lifetime (as assumed in the linear combination model). A characteristic localization time seems rather to be somewhere in between these two extremes.

5.6. Vacancies in Ice

The formation energy of water molecule vacancies, E_f, has been estimated to be about 0.5 eV. This value has been obtained on the assumption that it should be close to the sublimation energy[10,42]. With the relative vacancy concentration c given by

$$c = \exp(\frac{S_f}{k}) \exp(-\frac{E_f}{kT}) \qquad (27)$$

(S_f is the vacancy formation entropy, k Boltzmans constant and T the temperature), and on the assumtion that the entropy factor is approx. unity, c becomes about 10^{-10} close to the melting point for E_f = 0.5 eV. Thus the vacancy concentration in ice has generally been considered very low.

However, as mentioned in subsection 5.5 there is evidence from PAT investigations of γ-irradiated ice, and from self-diffusion results, that the vacancy concentration at the melting point is at least a few ppm[32,69]. We shall now discuss this further together with the present results.

In ref. 69 we showed that if self-diffusion in ice takes place by a vacancy mechanism, which seems to be generally accepted, the value of the diffusion constant D leads to a lower limit to the vacancy concentration. The average jump frequency of the molecules can be calculated from D. Only the four molecules at the vacancy can jump at a certain time with a frequency somewhat smaller than a typical phonon frequency. This puts the lower limit to the vacancy concentration, which appears to be a few ppm at the melting point[69]. Equation (27) then puts an upper limit to E_f for a given entropy factor. Using Zener's approximation for S_f[12,32,72], we find $E_f \lesssim 0.4$ eV (and $\exp(\frac{S_f}{k}) \leq 300$. For $\exp(\frac{S_f}{k}) \simeq 1$, we would get $E_f \lesssim 0.3$ eV).

In a recent paper we presented results of PAT investigations of the annealing behaviour of γ-irradiated ice[32]. A main conclusion was that the vacancy migration energy E_m = 0.34±0.07 eV, and hence E_f = 0.28±0.07 eV, because $E_f + E_m = Q$, the activation energy for diffusion that seems well determined at 0.62 eV[12,73]. This low E_f entails a vacancy concentration at the melting point of at least a few ppm.

The analysis of the present experimental data on Ps trapping in temperature-created vacancies showed that no simple model could convincingly account for the observations (subsection 5.5). Thus no detailed quantitative correlation can be obtained between the amount of Ps trapping and the vacancy concentration. On the other hand, the "trapping model with escape" suggested an $E_f \simeq 0.2$ eV, and using the linear combination model on the lifetime and angular correlation results separately gives E_f-values of 0.13-0.18 eV.

Another way to estimate E_f from the present measurements is to note that trapping of Ps sets in above about -100°C (Figs. 5-7 and ref. 18). Results on HF doped ice[18] showed that Ps trapping sets in at a relative defect concentration of 10^{-8} - 10^{-6} (similar to positron trapping in vacancies in metals that sets in at $c \sim 10^{-7}$). Using Zener's approximation for S_f[12,72] in eq. (27), we get $0.26 \text{ eV} < E_f < 0.35$ eV. (For $\exp(\frac{S_f}{k}) = 1$, $0.20 \text{ eV} < E_f < 0.28$ eV).

From the above discussion we can conclude that several independent experimental results lead to a number for the vacancy formation energy in ice between 0.2 and 0.3 eV, i.e. about half the previously assumed value, and as a consequence of this to a vacancy concentration close to the melting point of at least a few parts per million, i.e. more than 10^4 times higher than previously assumed. Furthermore, the present results suggest that a detectable divacancy concentration is present above approximately -40°C, i.e. $c_{2v} \gtrsim 10^{-7}$.

Information about vacancies in thermal equilibrium has mainly been obtained from diffusion[12] and NMR spin-lattice relaxation[73] measurements, which both give a value of 0.62 eV for the sum of the formation and migration energies. Possible aggregates of vacancies and Bjerrum defects have been considered[74-76], but Onsager and Runnels[75] argued against their existence. In accordance with this, possible interactions with vacancies seem not to have been included in the theories for ion state and Bjerrum defects[42,77], except for some short considerations by Seidenstticker and Longini[74]. They point out that, if the vacancy concentration is as high as parts per million, the influence of vacancies on the bulk Bjerrum defect population could be pronounced[74]. For instance, the question of the existence and possible configuration of D-defects in ice

has been a matter of extensive discussion[10,42] as the simple picture of two protons on a linear hydrogen bond is unrealistic because of its high energy. If the surroundings of the D-defect are allowed to relax, this energy is considerably reduced[10]. However, it seems that the space available in a vacancy might make a D-defect-vacancy aggregate energetically favourable. Thus, a high vacancy concentration may entail that almost all D-defects are bound to vacancies. The vacancy-D-defects bound state was apparently first introduced by Kopp[76].

Recently, Bilgram and Gränicher[77] revised the theory of Bjerrum and ion state defects and included interaction between the two types of electrically active defects. It now seems appropriate to go one step further and include interaction with vacancies too.

A number of different effects have been observed to take place in ice close to 100°K, e.g., in heat capacity[11], in electrical polarization and depolarization[11], in yield of trapped excess electrons[78], and recently annealing of the damage created by protons in channelling experiments[79]. With the demonstration in ref. 32 that vacancies migrate around this temperature, it seems worthwhile to consider the possible role of vacancy migration in these effects. In fact, this was partly done by Kawabata[78], who explained his results by assuming that electrons were trapped in radiation produced vacancies. In these traps the electrons absorb at wavelengths around 6400 Å, similar to the wavelengths of the absorption of hydrated electrons in water. We therefore propose that in these traps the surrounding water molecule dipoles have been oriented towards the vacancy in the same way as in water, where the molecules are oriented towards the hydrated electron, while the recently discovered infrared traps for electrons in ice[80,81] might be vacancies with no preferred orientation of the surrounding molecules.

5.7. Miscellaneous Remarks

In 1965 Colombino et al.[82] published angular correlation curves for polycrystalline ice at various temperatures between -144°C and 0°C. They found an apparently strong narrowing of the curves between -18°C and -25°C. On using our curves, we obtained a roughly similar, strong narrowing around -20°C - if we

normalized our curves to a standard height at the angles ± 4 mrad, as was done in ref. 82. Hence, this apparently strong narrowing is partly caused by the particular normalization used.

Mogensen et al.[19] made an error in their calculation of the expected fwhm of the narrow central peak. The Maxwellian velocity distribution for Ps contributes 0.49 mrad, not 0.25 mrad, at $T = 125^{\circ}K$. By use of fwhm = 0.24 mrad (0.3 mrad) for the finite slit width (uncertainty in sample height) contribution, as in ref. 19, we calculate fwhm = 0.63 mrad, while we measured fwhm = 0.72 mrad. However, the contribution from the uncertainty in the sample height was probably too low in ref. 19. A more realistic upper value of this contribution is 0.45 mrad (as used in section 2), which gives a fwhm = 0.71 mrad.

If we use fwhm = 0.65 mrad for the total geometric resolution (see section 2) and fwhm = $4.34 \cdot 10^{-2}\ T^{\frac{1}{2}}$ mrad (Maxwellian distribution) for the thermal smearing, we get

$$\text{fwhm} = (0.65^2 + 18.8 \cdot 10^{-4} \cdot T)^{\frac{1}{2}}$$

Hence, we get 0.77 mrad (0.97 mrad) at $-180^{\circ}C$ ($0^{\circ}C$), which is somewhat less than the measured values of 0.86 mrad (1.12 mrad) at $-180^{\circ}C$ ($0^{\circ}C$). Hence, the fwhm's of the central peaks seem to be significantly larger than expected, in particular at temperatures above $-50^{\circ}C$. Maybe this extra broadening is caused by a finite coherence length (finite size) of the Block function, which decreases for increasing temperature as a result of the increase in thermal motion of the atoms and in the disorder (defects) in the lattice. Divacancies may play a role here too. However, other explanations are possible, and hence we shall not pursue the interpretation here.

6. SUMMARY AND CONCLUSION

In this paper we have aimed to give a fairly complete discussion of the results of our studies of the behaviour of Ps in pure ice in the temperature interval $-180^{\circ}C \leq t \leq 2^{\circ}C$. Parts of the paper will constitute a basis for the discussion of similar results for HF-doped ice and other structures in several future papers.

At first we presented results of angular correlation measurements on monocrystals of light and heavy ice for various crystal orientations and as a function of temperature from $-182^{o}C$ to the melting point. The curves for temperatures below about $-100^{o}C$ consisted of a broad (fwhm ≈ 10.5 mrad) component and narrow (fwhm ≈ 1 mrad) central and side peaks. With increasing temperature above $-100^{o}C$ the intensities of the narrow peaks decreased followed by a simultaneous increase in intensity of a middle-broad (fwhm ≈ 3.9 mrad) component. These narrow and middle-broad components were interpreted as results of intrinsic para-Ps annihilation. The narrow components, which were positioned at angles equivalent to projections of reciprocal lattice points, gave evidence that the Ps is in a Bloch function state at low temperatures[19]. The middle-broad component was interpreted as resulting from localized para-Ps, the localization taking place at temperature-created water-molecule vacancies.

Also new results of positron lifetime measurements, which were more detailed than our previous measurements[18], were presented. Two longlived components were resolved in the analysis above $-60^{o}C$. The lifetime, τ_3, of one of them increased above $-60^{o}C$ from about 0.78 nsec to about 1.0 nsec at the melting point, its intensity being essentially constant $51 \pm 3\%$, in agreement with the results in ref. 18. The other,new component assumed to have a constant lifetime τ_4 = 1.7 nsec had an intensity, I_4, that was low below $-40^{o}C$, but increased sharply above $-40^{o}C$ from 1.5% to 5.1% at the melting point. Both longlived components were associated with pick-off annihilation of ortho-Ps, and we interpreted the increase of τ_3 with temperature as caused by localization of ortho-Ps at water molecule vacancies. The τ_4, I_4 component was tentatively interpreted as localization of ortho-Ps at divacancies.

Very detailed analysis methods were used in the interpretation of the data. Hence, the present paper included a rather extensive account of such methods, particularly for the angular correlation curves. The detailed analysis of these curves resulted in a determination of intensities and fwhm's of the narrow peaks and the middle-broad components in the temperature interval $-180^{o}C \lesssim t \lesssim 2^{o}C$ for the a- and c-axis oriented single crystals of ice. Hence, the components resulting from intrinsic para-Ps annihilation could be determined. In particular, the

components at various reciprocal lattice points resulting from intrinsic para-Ps annihilation from the Bloch function state were calculated. It turned out that the contributions at points different from the origin decreased faster than that of the origin for increasing temperature.

In a theoretical part of the paper a fairly general discussion of the annihilation of a Ps-many-electron system was given (section 4). Two new exchange terms in the annihilation probability were derived, and it was shown that the para-Ps pick-off rate is smaller than that of ortho-Ps. Furthermore, the influence of the thermal motion of the atoms on the Ps Bloch function, and hence on the narrow peaks in the angular correlation curves, was discussed. The narrow side peak intensity depends on the square of the Debye-Waller factor in the nearly-free-Ps approximation.

A detailed discussion followed of various aspects of the experimental angular correlation and lifetime results. The discussion made use of the theory outlined in section 4 and took into account the available results on Ps in ice and other systems.

At first, the existence of Ps was discussed. It was concluded that the experimental facts very strongly indicate that a Ps state is formed in ice. The total para-Ps formation, I_p, was found to be $I_p = 19.4\%$, on assuming that the para-Ps pick-off rate was equal to that measured for ortho-Ps. However, the ortho-Ps yield, I_3, has been found to be $I_3 = 54\%$ by use of the lifetime data. Hence $I_3 < 3I_p = 58.2\%$. Several possible reasons for this fact were mentioned.

As mentioned above different temperature dependences were found for the contributions from different reciprocal lattice points to the narrow peaks in the angular correlation curves. This difference could not be explained in terms of the nearly-free-Ps theory, i.e. in terms of the temperature dependence of the Debye-Waller factor. Several possible explanations were discussed.

An important part of the discussion concerned the influence of the presence of vacancies on the angular correlation and lifetime results. It was difficult to determine the detailed nature of the process of Ps localization on the vacancies. The main difficulty is associated with the fact that ortho-Ps and

para-Ps seem to be trapped to about the same degree at a given vacancy concentration, although ortho-Ps lives six times longer than para-Ps in the ice bulk. This cannot be explained in terms of the simple trapping model[3] normally used. An extended trapping model, which included the presence of divacancies and a probability of detrapping, fitted the data fairly well, but the fitting parameters were somewhat unrealistic. An alternative model, in which it was assumed that the Ps wave function is a linear combination of a Bloch function and a function localized on the monovacancies, did not explain the data in detail either. Of course, more elaborate models with many fitting parameters can explain the measured data by a variation of the parameters. We would like to emphasize the important fact that we could not explain the influence of the vacancies in terms of simple models. The basic idea of a trapping probability per unit time does not seem applicable in the case of Ps trapping in ice, except when using fairly elaborate models with many assumed processes. In this context, it is interesting to note that in cases of positron trapping in defects in metals and of electron trapping in defects in semiconductors and insulators, much less information on the trapping process is available compared to the case of Ps trapping in ice. Hence, we wonder whether the fact that the simplest possible model of trapping (i.e. a hypothesis of a trapping probability per unit time) is applicable to the positron and electron cases might be a result of the low level of information, and that this model would break down if more information, as in the case of Ps in ice, is available. Some indications that this might be the case for positron trapping in metals have recently be published[83].

Since we could not determine the exact nature of the influence of the vacancies on Ps behaviour, it was difficult to derive a very well-defined vacancy formation energy, E_f, from the data. However, irrespective of the model used, E_f was roughly 0.2 to 0.35 eV, which is much lower than the normally used value of 0.5 eV, and in agreement with the E_f-values derived from positron annihilation measurements on γ-irradiated[32] and HF-doped ice[31] and from self-diffusion measurements[69]. The smaller E_f-value means that the vacancy concentration must be several ppm at the melting point, i.e. 10^4 times higher than

normally[10,42] assumed. The higher vacancy concentration will probably imply a pronounced change in the normally accepted theories of the defects on the hydrogen bonds in ice, which presumably explain e.g. the dielectric properties of ice.

We believe, that the results presented in this and other, related papers, and the discussion given are of general interest from several points of view. First, the particular features of the annihilation process allow a direct determination of the Fourier transform of the Ps center-of-mass wave function. Such detailed information is not available for other particles (e.g. the electrons in Bloch function or trapped states). Secondly, Ps is in a Bloch function state in the defect-free ice. Apparently, Ps is the only atom shown to be in a Bloch function state. Thirdly, the change in the wave function due to the introduction of vacancies in ice, i.e. the change from a mainly delocalized to a mainly localized Ps state, has been studied. Fourthly, information on vacancies and polyvacancies in ice has been obtained. Very little is known about vacancies and polyvacancies in any molecular crystal.

Altogether, the results presented in this paper illustrate how very detailed information on the behaviour of Ps in a molecular crystal can be obtained. This information is of general importance for the understanding of the behaviour of the three light particles, the electron, the positron, and the Ps-atom in solids and liquids. Furthermore, the information can also shed new light on the behaviour of defects in molecular solids.

Added note. The authors of this paper participated in the Symposium on Physics and Chemistry of Ice, September 11-16, 1977 in Cambridge, England. Two short papers (O.E. Mogensen and M. Eldrup: Vacancies in Pure Ice Studied by Positron Annihilation Techniques and M. Eldrup, O.E. Mogensen and J. Bilgram: Vacancies in HF-doped and Irradiated Ice by Positron Annihilation Technique) were submitted. The proceedings (papers and discussions) will be published in Journal of Glaciology, volume 21, number 85.

ACKNOWLEDGEMENTS

The authors are indebted to G. Kvajić and J.H. Bilgram for providing the ice monocrystals. Discussions on the Ps Bloch function with A.R. Mackintosh, O. Krogh Andersen, and L.M. Falicov are gratefully acknowledged. Thanks are also due to N.J. Pedersen for valuable technical assistance.

REFERENCES

1) V.I. Goldanskii. At. Energy Rev. 6 No. 1 (1968) 3-148.

2) V.I. Goldanskii and V.G. Firsov. Annu. Rev. Phys. Chem. 22 (1971) 209-258.

3) R.N. West. Adv. Phys. 22 (1973) 263-383.

4) A.T. Stewart and L.O. Roellig (editors). Positron Annihilation. Proceedings of the Conference held at Wayne State University on July 27-29, 1965 (Academic Press, New York, 1967) 438 pp.

5) H.J. Ache. Angew. Chem. 84 (1972) 234-255.

6) J.A. Merrigan, J.H. Green, and S.J. Tao. In: Physical Methods of Chemistry edited by A. Weissberger and B.W. Rossiter Vol. 1, part 3D (Wiley, New York 1972) 501-586.

7) A. Seeger. J. Phys. F 3 (1973) 248-294.

8) K. Petersen, N. Thrane, and R.M.J. Cotterill. Philos. Mag. 29 (1974) 9-23.

9) S. Dannefær, G.W. Dean, and B.G. Hogg. Phys. Rev. B13 (1976) 3715-3723.

10) P.V. Hobbs, Ice Physics (Clarendon, Oxford, 1974) 837 pp.

11) E. Whalley, S.J. Jones and L.W. Gold (editors). Physics and Chemistry of Ice. Papers presented at the Symposium held in Ottawa, Canada, 14-18 August 1972 (Royal Society of Canada, Ottawa, 1973) 403 pp.

12) R.O. Ramseier. J. Appl. Phys. 38 (1967) 2553-2556.

13) H. Blicks, O. Dengel, and N. Riehl. Phys. Kondens. Mater. 4 (1966) 375-381.

14) P. Delibaltas, O. Dengel, D. Helmreich, N. Riehl, and H. Simon. ibid. 5 (1966) 166-170.

15) O. Dengel, E. Jacobs, and N. Riehl. ibid. 5 (1966) 58-59.

16) K. Itagaki. J. Phys. Soc. Jap. 19 (1964) 1081.

17) W. Kuhn and M. Thürkauf. Helv. Chim. Acta 41 (1958) 938-971.

18) M. Eldrup, O.E. Mogensen, and G. Trumpy. J. Chem. Phys. 57 (1972) 495-504.

19) O.E. Mogensen, G. Kvajić, M. Eldrup, and M. Milošević-Kvajić. Phys. Rev. B4 (1971) 71-73.

20) J.M. Ziman, Principles of the Theory of Solids. 2. ed. (Cambridge University Press, Cambridge, 1972) 435 pp.

21) W. Brandt, G. Coussot, and R. Paulin. Phys. Rev. Lett. 23 (1969) 522-524.

22) A. Greenberger, A.P. Mills, A. Thompson, and S. Berko. Phys. Lett. 32A (1970) 72-73.

23) C.H. Hodges, B.T.A. McKee, W. Triftshäuser, and A.T. Stewart. Can. J. Phys. 50 (1972) 103-109.

24) G. Coussot and R. Paulin. J. Appl. Phys. 43 (1972) 1325-1330.

25) G. Coussot. Phys. Lett. 30A (1969) 138-139.

26) G. Coussot, Ph. D. Thesis, (Faculté des Sciences d'Orsay, University of Paris, 1970) 142 pp.

27) T. Hyodo and Y. Takakusa. J. Phys. Soc. Japan 42 (1977) 1065-1066.

28) O.E. Mogensen and M. Eldrup,in: Ref. 11, p. 165-169.

29) M. Milošević-Kvajić, O.E. Mogensen, G. Kvajić, and M. Eldrup. J. Chem. Phys. 56 (1972) 2567-2571.

30) K. Petersen, M. Eldrup, and G. Trumpy. Phys. Lett. 31A (1970) 109-110.

31) M. Eldrup, O.E. Mogensen, and J. Bilgram, to be published.

32) M. Eldrup. J. Chem. Phys. 64 (1976) 5283-5290.

33) L. Smedskjær and G. Trumpy. Appl. Phys. 5 (1974) 49-52.

34) K.B. Hansen and P. Skaarup. Nucl. Instr. Meth. 65 (1968) 152-156.

35) M. Eldrup, O.E. Mogensen, and J.H. Evans. J. Phys. F6 (1976) 499-521.

36) J. Bilgram, in: Ref. 11, p. 246-250.

37) K. Higuchi, Acta Metall. 6 (1958) 636-642.

38) J. Bilgram, H. Wenzl, and G. Mair. J. Cryst. Growth 20 (1973) 319-321.

39) P. Kirkegaard and O.E. Mogensen, PAACFIT: a program for analysing positron annihilation angular correlation spectra. RISØ-M-1615 (1973) 25 pp.

40) P. Kirkegaard and M. Eldrup. Comput. Phys. Commun. 7 (1974) 401-409.

41) O.E. Mogensen and V.P. Shantarovich. Chem. Phys. 6 (1974) 100-108.

42) N.H. Fletcher. The Chemical Physics of Ice (Cambridge University Press, London, 1970) 271 pp.

43) O.E. Mogensen and V.P. Shantarovich, to be published.

44) O.E. Mogensen. J. Chem. Phys. 60 (1974) 998-1004.

45) O.E. Mogensen. Appl. Phys. 6 (1975) 315-322.

46) M. Eldrup, V.P. Shantarovich, and O.E. Mogensen. Chem. Phys. 11 (1975) 129-142.

47) P. Jansen, M. Eldrup, O.E. Mogensen, and P. Pagsberg. Chem. Phys. 6 (1974) 265-271.

48) B. Levay and O.E. Mogensen. J. Phys. Chem. 81 (1977) 373-377.

49) O.E. Mogensen. Electron Properties in Tin and Bismuth by Angular Correlation of Annihilation Photons. (Technical University of Denmark, København, 1968) 139 pp.

50) Chang Lee. Soviet Phys. - JETP 6 (1958) 281-291.

51) W.G. Wolfer and R.T. Schneider. On annihilation and other interactions of positrons in a plasma. AD 702406 (1970) 133 pp.

52) P.R. Wallace. Solid State Phys. 10 (1960) 1-69.

53) S. Kahana. Phys. Rev. 129 (1963) 1622-1630 and J. Crowell, V.E. Anderson, and R.H. Ritchie. Phys. Rev. 150 (1966) 243-248.

54) O.E. Mogensen. In: Preprints of the Fourth International Conference on Positron Annihilation, Helsingør, Denmark, 23-26 August 1976. Part 2, paper no. G3.

55) J.D. McGervey, in Ref. 4, p. 143-154.

56) P. Hautojærvi, M.T. Loponen, and K. Rytsölä. J. Phys. B9 (1976) 411-421.

57) R.V. Kasowski. Phys. Rev. 187 (1969) 891-901.

58) A.A. Maradudin, E.W. Montroll, G.H. Weiss, and I.P. Ipatova. Solid State Phys., Suppl. 3 (1971) 708 pp.

59) A.M. Stoneham. Theory of Defects in Solids (Clarendon, Oxford, 1975) 955 pp.

60) B.T.A. McKee, A.G.D. Jost, and I.K. MacKenzie. Can. J. Phys. 50 (1972) 415-420.

61) P. Colombino and B. Fiscella. Nuovo Cimento 3B (1971) 1-14.

62) M. Eldrup et al. (unpublished).

63) O.E. Mogensen. In: Preprints of the Fourth International Conference on Positron Annihilation, Helsingør, Denmark, 23-26 August 1976. Part 1, paper no. R10.

64) P. Jansen and O.E. Mogensen. Chem. Phys., in press.

65) J.M. Warman, private information.

66) J.A. Ghormley and A.C. Stewart. J. Amer. Chem. Soc. 78 (1956) 2934-2939.

67) P. Jansen, M. Eldrup, B. Skytte Jensen, and O.E. Mogensen. Chem. Phys. 10 (1975) 303-312.

68) S.W. Peterson and H.A. Levy. Acta Crystallogr. 10 (1957) 70-76.

69) O.E. Mogensen and M. Eldrup. Phys. Lett. 60A (1977) 325-326.

70) S. Dannefær, G.W. Dean, D.P. Kerr, and B.G. Hogg. Phys. Rev. B14 (1976) 2709-2714.

71) A. Seeger. Appl. Phys. 4 (1974) 183-199.

72) P.G. Shewmon. Diffusion in Solids (McGraw-Hill, New York 1963) 203 pp.

73) J.H. Bilgram, J. Roos, and H. Gränicher. Z. Phys. B23 (1976) 1-9.

74) R.G. Seidensticker and R.L. Longini. In: Physics of Ice. Proceedings, Munich, Germany, September 9-14, 1968. Edited by N. Riehl, B. Bullemer and H. Engelhardt (Plenum, New York, 1969) 471-482.

75) L. Onsager, L.K. Runnels. J. Chem. Phys. 50 (1969) 1089-1103.

76) M. Kopp, unpublished work, referred to in e.g. Refs. 73-74.

77) J.H. Bilgram and H. Gränicher. Phys. Condens. Matter 18 (1974) 275-291.

78) K. Kawabata. J. Chem. Phys. 65 (1976) 2235-2242.

79) I. Golechi, F. Rudolf, and C. Jaccard. Helv. Phys. Acta 49 (1976) 701-702.

80) G.V. Buxton, H.A. Gillis, and N.V. Klassen. Can. J. Chem. 55 (1977) 2385-2395.

81) H. Hase and K. Kawabata. J. Chem. Phys. 65 (1976) 64-67.

82) P. Colombino, B. Fiscella, and L. Trossi. Nuovo Cimento 38 (1965) 707-723.

83) S.C. Sharma, S. Berko, and W.K. Warburton. Phys. Lett. 58A (1976) 405-408.